Store-operated Ca^{2+} entry regulates Ca^{2+}-activated chloride channels and eccrine sweat gland function

Axel R. Concepcion,[1] Martin Vaeth,[1] Larry E. Wagner II,[2] Miriam Eckstein,[3] Lee Hecht,[1] Jun Yang,[1] David Crottes,[4] Maximilian Seidl,[5] Hyosup P. Shin,[1] Carl Weidinger,[1] Scott Cameron,[6] Stuart E. Turvey,[6,7] Thomas Issekutz,[8] Isabelle Meyts,[9] Rodrigo S. Lacruz,[3] Mario Cuk,[10] David I. Yule,[2] and Stefan Feske[1]

[1]Department of Pathology, New York University School of Medicine, New York, New York, USA. [2]Department of Pharmacology and Physiology, University of Rochester, Rochester, New York, USA. [3]Department of Basic Science and Craniofacial Biology, New York University College of Dentistry, New York, New York, USA. [4]Department of Physiology, UCSF, San Francisco, California, USA. [5]Department of Pathology, Institute for Surgical Pathology, University Medical Center, University of Freiburg, Freiburg, Germany. [6]Division of Allergy and Clinical Immunology, Department of Pediatrics, University of British Columbia, Vancouver, British Columbia, Canada. [7]British Columbia Children's Hospital and Child and Family Research Institute, Vancouver, British Columbia, Canada. [8]Division of Immunology, Department of Pediatrics, Dalhousie University, Halifax, Nova Scotia, Canada. [9]Department of Microbiology and Immunology, Department of Pediatrics, University Hospitals Leuven, KU Leuven, Leuven, Belgium. [10]Department of Pediatrics, Zagreb University Hospital Centre and School of Medicine, Zagreb, Croatia.

Eccrine sweat glands are essential for sweating and thermoregulation in humans. Loss-of-function mutations in the Ca^{2+} release–activated Ca^{2+} (CRAC) channel genes *ORAI1* and *STIM1* abolish store-operated Ca^{2+} entry (SOCE), and patients with these CRAC channel mutations suffer from anhidrosis and hyperthermia at high ambient temperatures. Here we have shown that CRAC channel–deficient patients and mice with ectodermal tissue–specific deletion of *Orai1* (*Orai1*^{K14Cre}) or *Stim1* and *Stim2* (*Stim1/2*^{K14Cre}) failed to sweat despite normal sweat gland development. SOCE was absent in agonist-stimulated sweat glands from *Orai1*^{K14Cre} and *Stim1/2*^{K14Cre} mice and human sweat gland cells lacking ORAI1 or STIM1 expression. In *Orai1*^{K14Cre} mice, abolishment of SOCE was associated with impaired chloride secretion by primary murine sweat glands. In human sweat gland cells, SOCE mediated by ORAI1 was necessary for agonist-induced chloride secretion and activation of the Ca^{2+}-activated chloride channel (CaCC) anoctamin 1 (ANO1, also known as TMEM16A). By contrast, expression of TMEM16A, the water channel aquaporin 5 (AQP5), and other regulators of sweat gland function was normal in the absence of SOCE. Our findings demonstrate that Ca^{2+} influx via store-operated CRAC channels is essential for CaCC activation, chloride secretion, and sweat production in humans and mice.

Introduction

Sweating is a physiological process primarily intended for thermoregulation in humans. Sweat is produced by eccrine sweat glands, which develop from the epidermal basal layer during embryogenesis (1). Each eccrine sweat gland is composed of 2 portions, the secretory coil and duct, which differ in structure and function (2). The secretory coil contains dark cells, clear cells, and myoepithelial cells, whereas the duct wall consists of a stratified cuboidal epithelium (2). Sweat secretion is mediated by a coordinated network of ion channels and transporters, which orchestrate the movement of Na^+ and Cl^- ions from the blood to the apical membrane of the secretory coil cells (3, 4). Increasing luminal salt concentrations establish an osmotic gradient that provides the driving force for the movement of water into the sweat gland lumen (5–7). Salt-enriched fluid produced by the secretory cells is collected in the ducts, which partially reabsorb Na^+ and Cl^- before the fluid is secreted via the sweat pore to reduce salt loss (1). Sweating is triggered in response to a variety of stimuli including heat as well as cholinergic and adrenergic agonists, which bind to muscarinic acetylcholine (ACh) receptors or α- and β-adrenergic receptors, respectively, that are expressed on secretory coil cells of sweat glands (8, 9). Reduced or abolished sweating is a rare human genetic condition referred to as hypohidrotic or anhidrotic ectodermal dysplasia (EDA, OMIM #305100), which in some cases occurs together with immunodeficiency (EDA-ID, OMIM #300291). Mutations in ectodysplasin A (*EDA*), its receptor ectodysplasin A receptor (*EDAR*), and the adaptor protein EDAR-associated death domain (*EDARADD*) cause EDA, whereas mutations in molecules of the nuclear factor κ light chain–enhancer of activated B cells (NF-κB) signaling pathway, NEMO (encoded by *IKBKG*) and IkBα (encoded by *NFKBIA*), are responsible for EDA-ID (10, 11). Anhidrosis is a serious medical problem particularly under conditions when sweating is required for thermoregulation, and may result in hyperthermia, stroke, and death (12, 13).

Sudorific agonists such as ACh increase the intracellular Ca^{2+} concentration ($[Ca^{2+}]_i$) (14–16). The resulting Ca^{2+} signals mediate the opening of Ca^{2+}-activated chloride channels (CaCCs) in secretory cells from different organs, including eccrine sweat glands (7, 17, 18). Several CaCCs, such as anoctamin 1 (ANO1, or TMEM16A) and bestrophin 2 (BEST2), have been reported to mediate fluid secretion in parotid acinar cells, submandibular salivary gland acinar cells, and colon and airway epithelia (19–23). In mice, targeted deletion of the *Best2* gene abolishes spontaneous sweat production

Authorship note: A.R. Concepcion and M. Vaeth contributed equally to this work.
Conflict of interest: S. Feske is a cofounder of Calcimedica.
Submitted: June 10, 2016; **Accepted:** August 31, 2016.
Reference information: *J Clin Invest*. 2016;126(11):4303–4318. doi:10.1172/JCI89056.

Table 1. Summary of patients with loss-of-function or null mutations in human *ORAI1* or *STIM1* genes that result in impaired SOCE and anhidrosis

Gene	Patient	Mutation	Protein	SOCE	Anhidrosis		Outcome	Reference
					Clinical	Sweat test		
ORAI1	1	p.R91W	+	–	Y	n.t.	Dead (11 mo)	McCarl et al. 2009 (35)
	2	p.R91W	+	–	Y	Y	Alive after HSCT (16 yr)	McCarl et al. 2009 (35)
	3	p.A88SfsX25	–	–	n.r.	n.t.	Dead (11 mo)	McCarl et al. 2009 (35)
	4	p.A103E/p.L194P	–	–	Y	Y	Dead (20 yr) after 2 HSCTs	McCarl et al. 2009 (35)
	5	p.H165PfsX1	–	residual	n.r.	n.t.	Alive after HSCT at 9 mo	Chou et al. 2015 (40)
	6	p.R270X	+	residual	n.r.	n.t.	Dead (7 mo)	Badran et al. 2016 (42)
	7	p.V181SfsX8	–	–	Y	Y	Alive after HSCT (8 yr)	Unpublished
	8	p.G98R	–	–	Y	Y	Alive after HSCT (20 mo)	Unpublished
	9	p.G98R	n.t.	n.t.	Y	Y	Dead (2.5 yr)	Unpublished
	10	p.L194P	–	–	Y	Y	Dead (7.5 mo)	Unpublished
STIM1	1	p.E128RfsX9	–	–	n.r.	n.t.	Dead (9 yr)	Picard et al. 2009 (36)
	2	p.E128RfsX9	–	n.t.	n.r.	n.t.	Alive after HSCT (6 yr)	Picard et al. 2009 (36)
	3	c.1538-1 G>A	–	–	n.r.	n.t.	Dead (2 yr)	Byun et al. 2010 (37)
	4	p.R429C	+	–	Y	Y	Alive after HSCT (6 yr)	Fuchs et al. 2012 (38)
	5	p.R429C	+	n.t.	Y	Y	Dead (21 mo)	Fuchs et al. 2012 (38)
	6	p.R426C	n.t.	n.t.	n.r.	n.t.	Lost to follow-up at 5 yr	Wang et al. 2014 (39)
	7	p.P165Q	+	–	Y	n.t.	Alive (8 yr)	Schaballie et al. 2015 (41)
	8	p.P165Q	+	–	Y	Y	Alive (21 yr)	Schaballie et al. 2015 (41)
	9	p.L74P	n.t.	–	Y	Y	Alive (11 yr)	Parry et al. 2016 (43)
	10	p.L74P	n.t.	–	Y	Y[A]	Alive (21 yr)	Parry et al. 2016 (43)
	11	p.L374P	+	–	Y	Y	Alive (22 yr)	Unpublished

[A]Hypohidrosis. HSCT, hematopoietic stem cell transplantation; n.r., not reported; n.t., not tested; p, protein; SOCE, store-operated Ca^{2+} entry; Y, yes.

in the absence of agonist stimulation (3, 24). In human eccrine sweat glands, the molecular nature of the CaCC responsible for chloride secretion is still debated (3). Also debated is the source of Ca^{2+} signals that activate CaCCs in eccrine sweat glands (3). Ca^{2+} release from the endoplasmic reticulum (ER) through inositol 1,4,5-trisphosphate receptors (IP_3Rs) and the subsequent increase in $[Ca^{2+}]_i$ have recently been shown to be required for eccrine sweat gland function, as patients with mutations in the type 2 IP_3R were anhidrotic (16). By contrast, earlier studies had shown that Ca^{2+} influx from the extracellular space is essential for sweating in response to cholinergic and α-adrenergic stimulation (14). However, the channels mediating Ca^{2+} influx in secretory sweat gland cells and the mechanism by which these channels regulate sweat secretion remain unknown (25).

Store-operated Ca^{2+} entry (SOCE) is a universal Ca^{2+} influx mechanism in a large variety of cell types (26). It is mediated by the activation of Ca^{2+} release–activated Ca^{2+} (CRAC) channels that are composed of ORAI1, and potentially ORAI2 and ORAI3, subunits localized in the plasma membrane (PM). CRAC channels are activated following agonist stimulation of cell surface receptors such as the G protein–coupled ACh receptor. Its engagement results in activation of phospholipase C, production of IP_3, and opening of IP_3Rs in the ER membrane that function as Ca^{2+} release channels (27). Ca^{2+} release from ER stores and the subsequent reduction of the ER Ca^{2+} concentration ($[Ca^{2+}]_{ER}$) lead to the activation of the ER membrane proteins stromal interaction molecule 1 (STIM1) and STIM2 via the dissociation of Ca^{2+} from EF hand motifs in the ER luminal N-termini of STIM1 and STIM2 (26, 28). Once activated, both proteins translocate to ER-PM junctions where they bind to and open ORAI1-CRAC channels that mediate the sustained Ca^{2+} influx from the extracellular space, which is required for many cell functions. The importance of CRAC channels is evident in human patients with autosomal recessive loss-of-function or null mutations in *ORAI1* and *STIM1* genes that abolish SOCE. These patients present with a unique syndrome, termed CRAC channelopathy, which is characterized by severe immunodeficiency, autoimmunity, congenital muscular hypotonia, and EDA. Besides anhidrosis, EDA in these patients is characterized by defects in dental enamel formation (29, 30). Although studies of human patients with CRAC channelopathy and mice with conditional deletion of *Orai1*, *Stim1*, and *Stim2* genes have greatly increased our understanding of the physiological role of CRAC channels and how they regulate the function of the immune system and other organs (31), their role in sweat glands remains largely undefined.

We show here that deletion of CRAC channels and SOCE abolish the function, but not the development, of eccrine sweat glands, resulting in anhidrosis, in both human and mice. We demonstrate that Ca^{2+} influx in response to agonist stimulation of eccrine sweat glands depends on ORAI1, STIM1, and STIM2, which are required for the activation of CaCCs and Cl^- secretion. Our results identify TMEM16A as the CaCC in human sweat gland cells and SOCE as a conserved Ca^{2+} influx pathway that is critical for CaCC function, sweat secretion, and thermoregulation.

Results

Anhidrosis in SOCE-deficient patients despite normal development of eccrine sweat glands. Mutations in different components of the

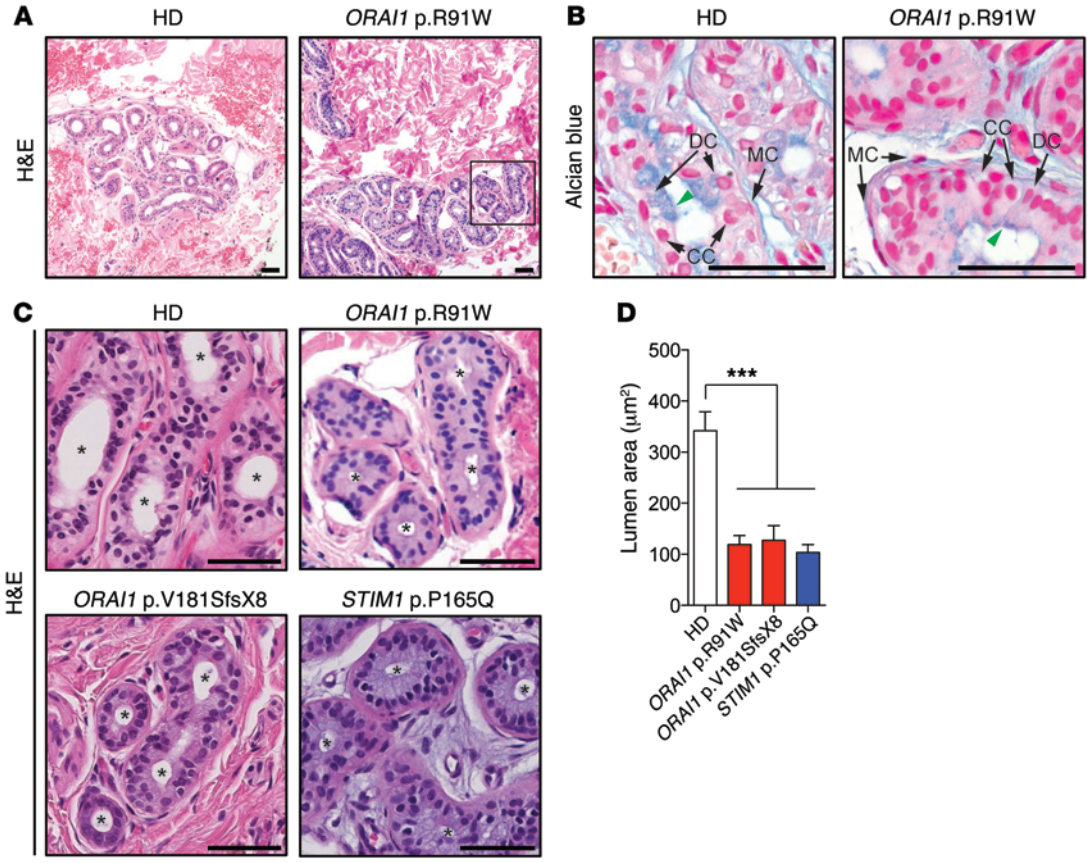

Figure 1. Sweat glands are present in CRAC channel–deficient patients with EDA-ID. (**A**) H&E staining of eccrine sweat glands in the dermis of a healthy control donor (HD) and a patient with *ORAI1* p.R91W loss-of-function mutation at low magnification. (**B**) Alcian blue staining of the same biopsies shown in **A** to detect acid mucopolysaccharides in dark cells (green arrowheads). Arrows indicate different cell types in the secretory portion of sweat glands (CC, clear cells; DC, dark cells; and MC, myoepithelial cells). (**C**) H&E staining of eccrine sweat glands in the dermis of an HD and patients with *ORAI1* p.R91W (magnification of boxed area in **A**), *ORAI1* p.V181SfsX8, and *STIM1* p.P165Q mutations that abolish SOCE. Asterisks indicate the lumen of secretory sweat glands. Scale bars in **A**–**C**: 50 μm. (**D**) Quantification of sweat gland lumens from human skin biopsies shown in **C**. Bars represent the means of 3 HDs and 3 individual patients. Between 2 and 4 coiled nests of eccrine sweat glands were analyzed per skin biopsy. Statistical analyses were performed by 1-way ANOVA using HDs as a reference and multiple comparisons. ***$P < 0.001$.

NF-κB signaling pathway were shown to cause EDA-ID (32, 33). Affected patients have abnormal development of ectodermal tissues including the skin, hair, teeth, and sweat glands. Most patients have fewer sweat glands, accounting for their anhidrosis (34). The EDA-ID phenotype is reminiscent of patients with CRAC channelopathy caused by loss-of-function or null mutations in *ORAI1* or *STIM1*, who also present with EDA-ID and tooth defects (30). However, their immunodeficiency is caused predominantly by T cell dysfunction, and their tooth defect is characterized by reduced enamel calcification in contrast to small, conical teeth in patients with defective NF-κB signaling. Hypohidrosis or anhidrosis has been found in all patients with mutations in *ORAI1* and *STIM1* when sweat secretion was tested directly by iontophoresis, and was present clinically in most patients as an overt inability to sweat at high ambient temperatures and/or hyperthermia (Table 1) (35–43). To investigate whether anhidrosis in CRAC channel–deficient patients was due to abnormal development of sweat glands as in other patients with EDA-ID, we analyzed skin biopsies from patients with mutations in *ORAI1* and *STIM1* that abolish SOCE. Eccrine sweat glands were present in the dermis of a patient homozygous for an *ORAI1* p.R91W loss-of-function mutation (44), an *ORAI1* p.V181SfsX8 null mutation that abolishes *ORAI1* expression, and a *STIM1* p.P165Q loss-of-function mutation (41) (Table 1 and Figure 1, A–C). None of the 3 patients was able to sweat when tested by iontophoresis following cutaneous pilocarpine stimulation, similar to other patients with mutations in *ORAI1* (p.G98R, p.L194P, or compound p.A103E/p.L194P) and *STIM1* (p.R429C, p.L374P, or p.L74P) that abolish SOCE (Table 1). The morphology of sweat glands of all 3 investigated CRAC channel–deficient patients appeared largely normal and similar to that of healthy donor controls (Figure 1, A–C). Different cell types that constitute eccrine sweat glands, including clear cells, dark cells, and myoepithelial cells, were visible histologically in biopsies of the CRAC channel–deficient patients (Figure 1, B and C). The main morphological difference we observed in patient samples compared with healthy donors was a significantly reduced sweat gland lumen (Figure 1, C and D), which is likely due to impaired sweat secretion. Consistent with this interpretation, we found fewer granula-containing acid mucopolysaccharides in the apical cytoplasm of sweat gland cells from an ORAI1-deficient patient

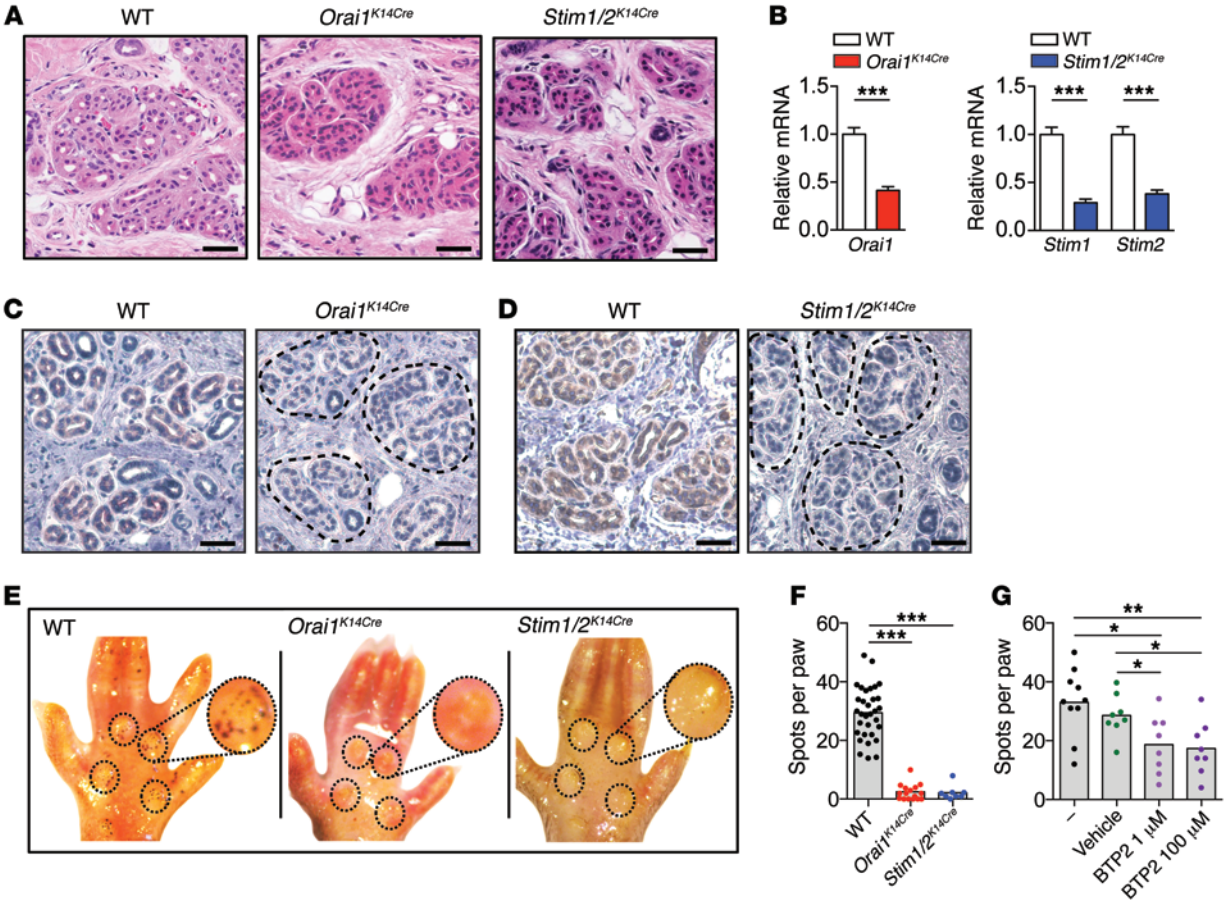

Figure 2. Deletion of *Orai1* or *Stim1/Stim2* in murine sweat glands abolishes sweating. (**A**–**D**) Analysis of sweat gland morphology in *Orai1* and *Stim1/2*-deficient mice. (**A**) H&E staining of hind paw skin biopsies of WT, $Orai1^{K14Cre}$, and $Stim1/2^{K14Cre}$ mice. Images are representative of 8 WT, 4 $Orai1^{K14Cre}$, and 4 $Stim1/2^{K14Cre}$ mice. Scale bars: 50 μm. (**B**) *Orai1* (left) and *Stim1* and *Stim2* (right) mRNA expression in sweat glands isolated from paws of WT ($n = 14$), $Orai1^{K14Cre}$ ($n = 7$), and $Stim1/2^{K14Cre}$ ($n = 10$) mice analyzed by quantitative real-time PCR. *Hprt* was used to normalize mRNA expression levels. Data are shown relative to mRNA levels in WT and as mean ± SEM. Statistical analysis by 2-tailed Student's *t* test. $^{***}P < 0.001$. (**C** and **D**) Immunohistochemical staining of ORAI1 (**C**) and STIM1 (**D**) in eccrine sweat glands in footpads of WT, $Orai1^{K14Cre}$, and $Stim1/2^{K14Cre}$ mice. Images are representative of 2 mice per genotype. Scale bars: 50 μm. (**E**–**G**) Impaired sweating in *Orai1* and *Stim1/2*-deficient mice. ACh induced sweat responses in the hind paws of WT, $Orai1^{K14Cre}$, and $Stim1/2^{K14Cre}$ mice. The paws of mice were coated with starch-iodine solution and injected s.c. with 100 μM ACh, and sweat dots were counted 5 minutes afterward. (**E**) Representative images. (**F**) Averaged number of sweat dots on the paws of 16 WT, 8 $Orai1^{K14Cre}$, and 4 $Stim1/2^{K14Cre}$ mice. Each dot represents 1 hind paw from an individual mouse. (**G**) ACh induced sweat responses in the hind paws of WT mice that were pretreated epicutaneously with 1 μM or 100 μM CRAC channel inhibitor BTP2 or vehicle (ethanol) 4 hours and 2 hours before ACh injection. Each dot represents 1 hind paw from an individual mouse. Statistical analyses in **F** and **G** were performed by 1-way ANOVA using multiple comparisons. $^{*}P < 0.05$, $^{**}P < 0.01$, $^{***}P < 0.001$.

compared with a healthy donor identified by Alcian blue staining, suggesting impaired function of dark cells of sweat glands (45). Collectively, these data indicate that anhidrosis in CRAC channel–deficient patients is not due to impaired eccrine sweat gland development but is instead a defect in their secretory function.

Deletion of Orai1 or Stim1/Stim2 genes in murine sweat glands abolishes sweating despite normal sweat gland development. In contrast to humans, eccrine sweat glands in mice are found only in the footpads. We first investigated whether CRAC channel genes are present in sweat glands of WT mice. *Orai1* and *Stim1* mRNA was highly expressed, whereas transcript levels of *Orai2*, *Orai3*, and *Stim2* were less abundant (Supplemental Figure 1A; supplemental material available online with this article; doi:10.1172/JCI89056DS1). To study the role of CRAC channels in murine eccrine sweat glands, we generated mice with conditional deletion of CRAC channel genes in tissues of ectodermal origin, including skin, teeth, and sweat glands. Histological analysis of eccrine sweat glands in the footpads of $Orai1^{fl/fl}$ *K14-Cre* (hereafter referred to as $Orai1^{K14Cre}$) and $Stim1^{fl/fl}$ $Stim2^{fl/fl}$ *K14-Cre* (hereafter referred to as $Stim1/2^{K14Cre}$) mice showed glands with a morphology similar to that in WT control mice with the exception of significantly smaller sweat gland lumens (Figure 2A and Supplemental Figure 1, B–D), thus resembling the findings in human patients with CRAC channelopathy. *Orai1* and *Stim1/Stim2* mRNA expression was substantially reduced in sweat glands isolated from $Orai1^{K14Cre}$ and $Stim1/2^{K14Cre}$ mice, respectively (Figure 2B). The residual mRNA levels observed are likely due to contamination of sweat gland tissue with other cells in the footpad preparation that are not of ectodermal origin and do not express keratin 14. This interpretation is supported by the complete lack of ORAI1 and STIM1 protein observed by immunohistochemistry in eccrine sweat glands of $Orai1^{K14Cre}$ and $Stim1/2^{K14Cre}$ mice compared with WT controls,

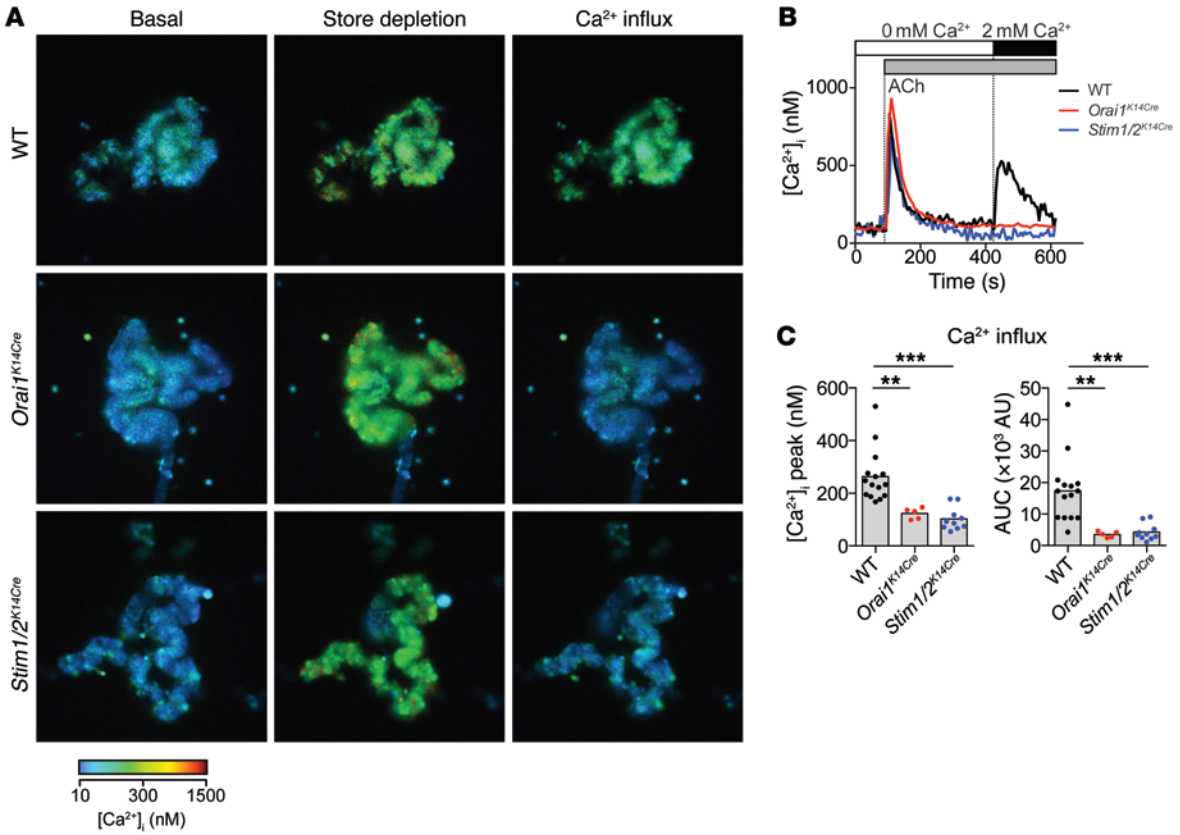

Figure 3. Deletion of *Orai1* or *Stim1/Stim2* in murine sweat glands abolishes SOCE. (**A**–**C**) Sweat glands isolated from the footpads of WT (top), *Orai1*^{K14Cre} (middle), and *Stim1/2*^{K14Cre} (bottom) mice were loaded with CellTracker Orange (CMRA) and Fura-2 for 30 minutes. Intracellular Ca^{2+} levels were determined by time-lapse microscopy of F340/F380 values that were calibrated to $[Ca^{2+}]_i$. (**A**) Representative F340/F380 ratios before stimulation in Ca^{2+}-free buffer ("basal"), after stimulation with 1 μM ACh in Ca^{2+}-free buffer ("store depletion"), and after perfusion with 2 mM Ca^{2+} ("Ca^{2+} influx"). (**B**) Representative traces of $[Ca^{2+}]_i$ from an experiment similar to the one shown in **A**. (**C**) Averaged peak $[Ca^{2+}]_i$ (left) and integrated Ca^{2+} response (area under the curve, AUC, right) after readdition of 2 mM Ca^{2+} (420–600 seconds). Bars represent the mean of 15 WT, 5 *Orai1*^{K14Cre}, and 10 *Stim1/2*^{K14Cre} mice. Each dot represents data from 1 gland of an individual mouse. Statistical analyses in **C** were performed by 1-way ANOVA followed by Bonferroni post hoc test. $^{**}P < 0.01$, $^{***}P < 0.001$.

which show strong ORAI1 and STIM1 expression (Figure 2, C and D). Together, mice with conditional deletion of CRAC channel genes in ectodermal tissues have sweat glands of largely normal morphology with the exception of reduced sweat gland lumens.

We next investigated the effects of CRAC channel deletion on eccrine sweat gland function by inducing sweat secretion in WT, *Orai1*^{K14Cre}, and *Stim1/2*^{K14Cre} mice via cholinergic stimulation (46). Since innervated sweat glands are restricted to the footpads in mice (47), we tested sweat secretion in the hind paws of mice, which were painted with iodine-starch solution and injected s.c. with ACh. Analyzing the number of dark spots on the paw surface, which correspond to active sweat pores, 5 minutes after ACh treatment, we found about 30 spots per paw in WT mice but hardly any spots in *Orai1*^{K14Cre} and *Stim1/2*^{K14Cre} mice (Figure 2, E and F), indicating that CRAC channels are required for eccrine sweat gland function in mice. It is noteworthy that while *Orai2* mRNA expression was detected in sweat gland tissue from WT mice (Supplemental Figure 1A), we did not observe a defect in sweat secretion in *Orai2*$^{-/-}$ mice (Supplemental Figure 2), suggesting that ORAI1 is the main CRAC channel homolog mediating SOCE in eccrine sweat gland cells. We next tested the effects of acute CRAC channel inhibition on sweat secretion by epicutaneous application of the CRAC channel inhibitor BTP2 to the footpads of WT mice. BTP2 treatment resulted in a significant reduction in sweat production over a 100-fold concentration range (Figure 2G). Taken together with the findings in mice with conditional deletion of *Orai1* and *Stim1/2* genes, these data suggest that CRAC channels regulate the function, but not the development, of murine eccrine sweat glands.

ORAI1, STIM1, and STIM2 mediate agonist-induced Ca^{2+} influx in sweat glands but are not required for expression of ion channels mediating Cl^- secretion. To assess the role of ORAI1, STIM1, and STIM2 in Ca^{2+} signaling in response to agonist stimulation of eccrine sweat glands, we isolated individual glands from the paws of *Orai1*^{K14Cre} or *Stim1/2*^{K14Cre} mice and analyzed them for $[Ca^{2+}]_i$. Stimulation with ACh in Ca^{2+}-free media induced a comparable Ca^{2+} release from ER stores in the secretory coils of sweat glands of WT and *Orai1*- and *Stim1/2*-deficient mice (Figure 3, A and B, and Supplemental Figure 3). Readdition of extracellular Ca^{2+} caused robust Ca^{2+} influx in sweat glands of WT but not *Orai1*^{K14Cre} or *Stim1/2*^{K14Cre} mice (Figure 3, A–C), indicating that ORAI1 and STIM1/2 mediate SOCE in murine eccrine sweat glands upon cholinergic stimulation. While Ca^{2+} entry following ACh stimulation could potentially be mediated by channels other than CRAC, this

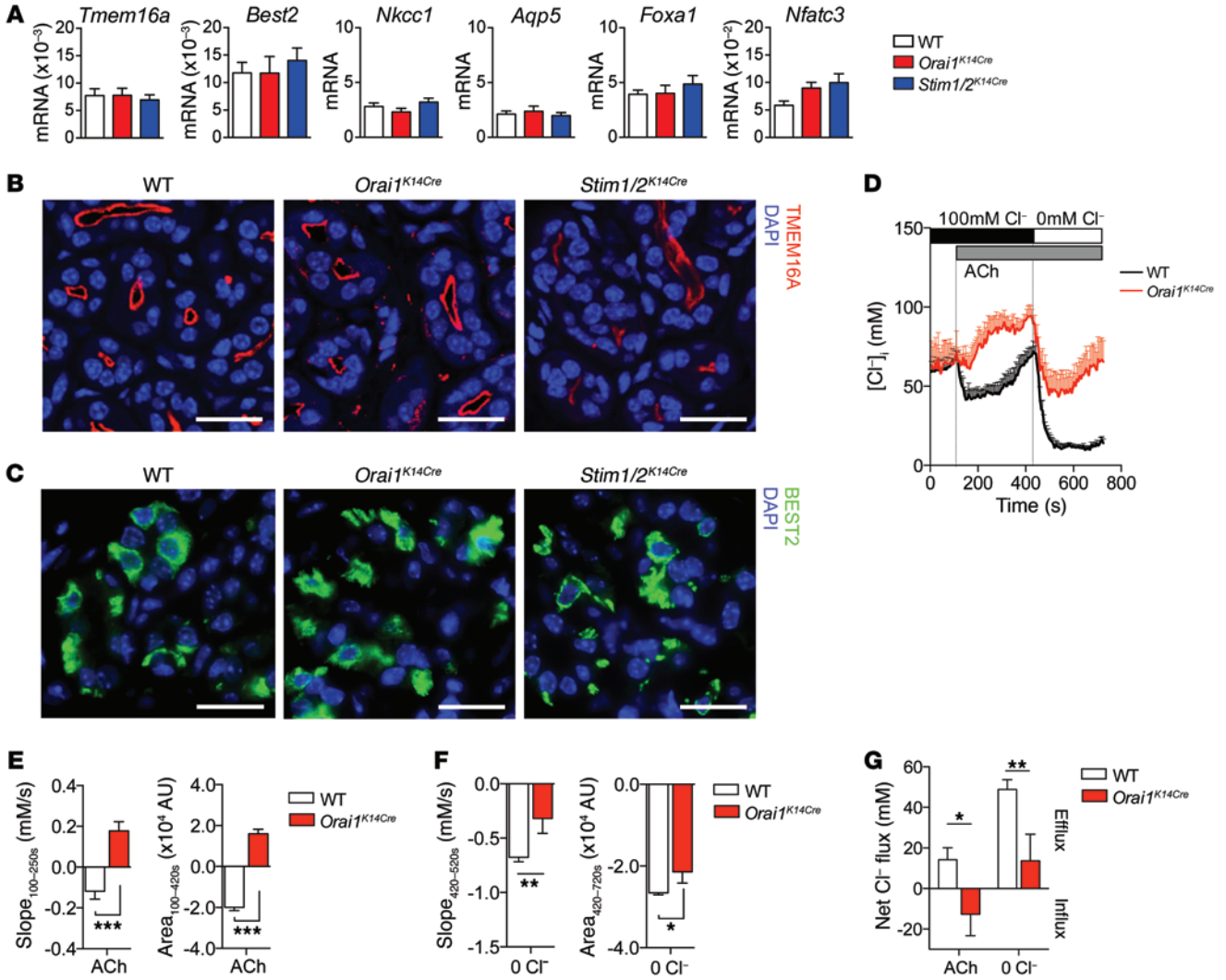

Figure 4. SOCE regulates Cl^- secretion in murine sweat glands. (**A**) mRNA expression of *Tmem16a, Best2, Nkcc1, Aqp5, Foxa1* and *Nfatc3* was analyzed by quantitative real-time PCR from sweat glands isolated from the paws of 14 WT, 7 *Orai1*^{K14Cre} and 10 *Stim1/2*^{K14Cre} mice. *Hprt* was used to normalize mRNA expression levels. (**B** and **C**) Protein expression and localization of TMEM16A (**B**) and BEST2 (**C**) by immunofluorescence. Eccrine sweat glands in the hind paws of WT, *Orai1*^{K14Cre} and *Stim1/2*^{K14Cre} mice were stained with antibodies against TMEM16A (red, in **B**), BEST2 (green, in **C**) and nuclei were counterstained with DAPI (blue, in **B** and **C**). Representative images of 2 mice per genotype. Scale bars: 20 μm. (**D**–**G**) Measurements of intracellular Cl^- concentrations ($[Cl^-]_i$) in eccrine sweat glands isolated from WT and *Orai1*^{K14Cre} mice. Sweat glands were loaded with MQAE and stimulated with 1 μM ACh in buffer containing 100 mM Cl^- followed by perfusion with Cl^--free buffer ("0 mM Cl^-") to force Cl^- secretion. MQAE signals were calibrated to absolute $[Cl^-]_i$. (**D**) $[Cl^-]_i$ traces represented as mean ± SEM of glands isolated from 11 WT and 7 *Orai1*^{K14Cre} mice. (**E**) Quantification of the Cl^- flux rate ("slope$_{100\text{-}250s}$") and change of $[Cl^-]_i$ measured as integrated area ("area$_{100\text{-}420s}$", relative to baseline) after stimulation with 1 μM ACh. (**F**) Quantification of the Cl^- flux rate ("slope$_{420\text{-}520s}$") and change of $[Cl^-]_i$ measured as integrated area ("area$_{420\text{-}720s}$", relative to baseline) after removal of extracellular Cl^-. (**G**) Quantification of net Cl^- efflux calculated as the difference between $[Cl^-]_i$ at the beginning of the experiment and after stimulation with 1 μM ACh, or after removal of extracellular Cl^- at the end of the experiment, respectively. For additional details see Supplemental Methods. Data in **E**–**G** are the mean ± SEM of 11 WT and 7 *Orai1*^{K14Cre} mice. Statistical analysis by 2-tailed Student's *t* test. $^*P < 0.05$, $^{**}P < 0.01$, $^{***}P < 0.001$.

is unlikely given the fact that deletion of either *Orai1* or *Stim1/2* resulted in a similar Ca^{2+} influx defect.

To understand the mechanisms underlying the sweating defect in CRAC channel–deficient mice and patients, we first tested whether SOCE controls the expression of molecules that mediate Cl^- and water secretion by eccrine sweat glands. In mice, the CaCC BEST2 is required for sweat production, as its deletion in *Best2*$^{-/-}$ mice causes severe hypohidrosis (3, 24). Based on studies in the NCL-SG3 sweat gland cell line, TMEM16A has been implicated as a molecular component of CaCCs in human eccrine sweat glands (7). Besides BEST2 and TMEM16A, the intracellular Cl^- concentration ($[Cl^-]_i$) in sweat gland cells is regulated by the electroneutral Na^+-K^+-2Cl^- cotransporter NKCC1 (encoded by the *SLC12A2* gene), which mediates Cl^- influx across the basolateral membrane of secretory cells (24, 48, 49). Cl^- secreted via CaCCs into the sweat gland lumen results in the consecutive secretion of water into the acini lumen mediated by the opening of the water channel aquaporin 5 (AQP5) (5). Expression levels of *Best2* and *Tmem16a* mRNA and BEST2 and TMEM16A protein as analyzed by immunofluorescence were normal in eccrine sweat glands iso-

lated from *Orai1*^{K14Cre} and *Stim1/2*^{K14Cre} mice compared with WT controls (Figure 4, A–C). As expected, TMEM16A was mainly localized in the apical membrane of secretory sweat glands (Figure 4B and Supplemental Figure 4), whereas BEST2 was distributed throughout the cytoplasm (Figure 4C), consistent with findings in a previous study (24). Furthermore, we found normal levels of *Nkcc1* and *Aqp5* mRNA in sweat glands from *Orai1*^{K14Cre} and *Stim1/2*^{K14Cre} mice (Figure 4A). Expression of other Cl^--permeable channels and transporters such as TMEM16B, CFTR, and NKCC2 that might contribute to Cl^- transport and sweating was very low and barely detectable by quantitative real-time PCR (data not shown). Normal transcript levels of Cl^- channels and transporters are consistent with normal expression of the transcription factors FOXA1, which was shown to regulate the expression of BEST2 and NKCC1 (24), and NFATc3, which is regulated by Ca^{2+} signals and activates FOXA1 (50) (Figure 4A). Collectively, these data show that impaired sweat secretion in CRAC channel–deficient mice is not due to abnormal expression of the CaCCs BEST2 and TMEM16A or other channels that regulate Cl^- and water secretion.

SOCE mediates Cl^- secretion in mouse and human sweat gland cells. We next tested the functional role of SOCE in Cl^- secretion by primary murine sweat glands. Isolated sweat glands from WT and *Orai1*^{K14Cre} mice were loaded with the intracellular Cl^- indicator MQAE and stimulated with ACh in buffer containing physiological Ca^{2+} (2 mM) and Cl^- (100 mM) concentrations followed by removal of extracellular Cl^- to force Cl^- secretion (Figure 4D). Before stimulation, WT and *Orai1*-deficient sweat glands had comparable $[Cl^-]_i$ (WT: 62 ± 12 mM; *Orai1*^{K14Cre}: 61 ± 8 mM). After ACh stimulation, $[Cl^-]_i$ significantly decreased in WT glands consistent with Cl^- secretion (Figure 4, D and E). By contrast, sweat glands from *Orai1*^{K14Cre} mice showed a moderate increase in $[Cl^-]_i$, which suggests a predominance of Cl^- influx mechanisms in the absence of Cl^- secretion. When extracellular Cl^- was replaced with isethionate to force Cl^- secretion from cells, WT sweat glands showed a strong reduction of $[Cl^-]_i$ consistent with Cl^- efflux as expected (Figure 4, D and F). *Orai1*^{K14Cre} sweat glands also showed reduced $[Cl^-]_i$, but the decrease was much less pronounced compared with that in WT cells. There was a striking difference in the overall net reduction of $[Cl^-]_i$ at the end of experiments compared with baseline $[Cl^-]_i$ in WT sweat gland cells (~50 mM), whereas only a small decrease in *Orai1*^{K14Cre} cells was observed (~10 mM) (Figure 4G). The residual reduction in $[Cl^-]_i$ in *Orai1*^{K14Cre} sweat glands after removal of extracellular Cl^- is likely due to Ca^{2+}-independent Cl^- efflux mechanisms that are preserved in ORAI1-deficient cells. These results demonstrate that SOCE is required to mediate Cl^- secretion in murine eccrine sweat glands.

To test whether human sweat glands also require SOCE for Cl^- secretion, we used the human eccrine sweat gland cell line NCL-SG3 (51), which has been widely used to measure epithelial ion transport (7, 51, 52). NCL-SG3 cells abundantly expressed *ORAI1* and *STIM1* mRNA (data not shown) and protein (Supplemental Figure 5, A–C). Suppression of ORAI1 and STIM1 in NCL-SG3 cells by shRNA strongly reduced their mRNA (Figure 5A) and protein (Supplemental Figure 5, A–C) expression. We found strongly reduced SOCE in NCL-SG3 cells stably transduced with shORAI1 and shSTIM1 after ionomycin stimulation, whereas Ca^{2+} release from ER stores was unaffected (Figure 5, B and C), indicating that ORAI1 and STIM1 regulate SOCE in human sweat gland cells.

We next analyzed $[Cl^-]_i$ in NCL-SG3 cells lacking ORAI1 or STIM1 expression following induction of SOCE. One particular characteristic of NCL-SG3 cells is their inability to respond to cholinergic stimulation with ACh (17, 51, 53, 54). They do, however, have anion fluxes in response to the Ca^{2+} ionophores calcimycin and ionomycin (17, 54). Ionomycin stimulation of NCL-SG3 cells in 100 mM $[Cl^-]_o$ (where $[Cl^-]_o$ indicates the extracellular concentration of Cl^-) resulted in a moderate reduction of $[Cl^-]_i$, which was strongly enhanced when Cl^- secretion was forced by removal of Cl^- from the extracellular buffer (Figure 5, D and E). NCL-SG3 cells transduced with shORAI1 or shSTIM1 lacked a comparable reduction of $[Cl^-]_i$, suggesting that Cl^- secretion by NCL-SG3 cells depends on SOCE (Figure 5, D and E). Defective Cl^- secretion in SOCE-deficient NCL-SG3 cells was not due to altered expression of CaCCs, since the reduction of SOCE by shORAI1 or shSTIM1 did not decrease *TMEM16A* and *BEST2* mRNA levels (Figure 5F). These results are consistent with our findings in murine sweat glands and demonstrate that SOCE is a conserved mechanism for Cl^- secretion in eccrine sweat glands.

SOCE is required for activation of CaCCs in human sweat glands. To characterize the mechanism by which SOCE regulates Cl^- secretion, we measured Cl^- currents in NCL-SG3 cells. Using the whole-cell patch-clamp configuration, we observed that Cl^- currents are activated in the presence of 1 μM Ca^{2+} in the patch pipette, and thus the cytosol, whereas no Cl^- currents were observed in the absence of Ca^{2+} (Figure 6, A and B). The Cl^- currents displayed hallmarks of epithelial CaCC currents, including fast activation followed by a smaller slow time-dependent component, deactivating tail currents upon repolarization (Figure 6B), and strong outward rectification (Figure 6C). CaCC currents with similar properties were detected in SOCE-deficient NCL-SG3 cells after transduction with shORAI1 when the patch pipette contained 1 μM Ca^{2+} (Figure 6, B and C). These results show that ORAI1-deficient NCL-SG3 cells can activate CaCC currents similarly to SOCE-sufficient NCL-SG3 cells when cytosolic $[Ca^{2+}]$ is elevated directly through the patch pipette, thus confirming the presence of functional CaCCs in NCL-SG3 cells. Stimulation of WT NCL-SG3 cells with ionomycin in the presence of extracellular Ca^{2+}, which depletes ER Ca^{2+} stores and induces SOCE (Figure 5B), resulted in robust and sustained Cl^- currents (Figure 6, D and E). The currents had properties similar to those induced by inclusion of 1 μM Ca^{2+} in the patch pipette (Figure 6, B and C) and were consistent with reported CaCC currents (23, 55). By contrast, ORAI1-deficient NCL-SG3 cells showed only transient and attenuated Cl^- currents upon ionomycin stimulation (Figure 6, D and E). Transient Cl^- currents parallel the transient increase in $[Ca^{2+}]_i$ resulting from ER Ca^{2+} release in the absence of SOCE in ORAI1-deficient cells (Figure 5B), indicating that SOCE is required for sustained activation of CaCCs, whereas Ca^{2+} release from ER stores can only transiently and partially activate CaCCs.

To investigate whether SOCE is required for CaCC function in agonist-stimulated sweat glands, we treated WT and ORAI1-deficient NCL-SG3 cells with trypsin, an agonist of proteinase-activated receptor 2 (PAR2), which has previously been shown to evoke CaCC currents in NCL-SG3 cells (56). Stimulation of WT NCL-SG3 cells with trypsin in Ca^{2+}-containing media resulted in stronger and more sustained elevation of $[Ca^{2+}]_i$ in comparison

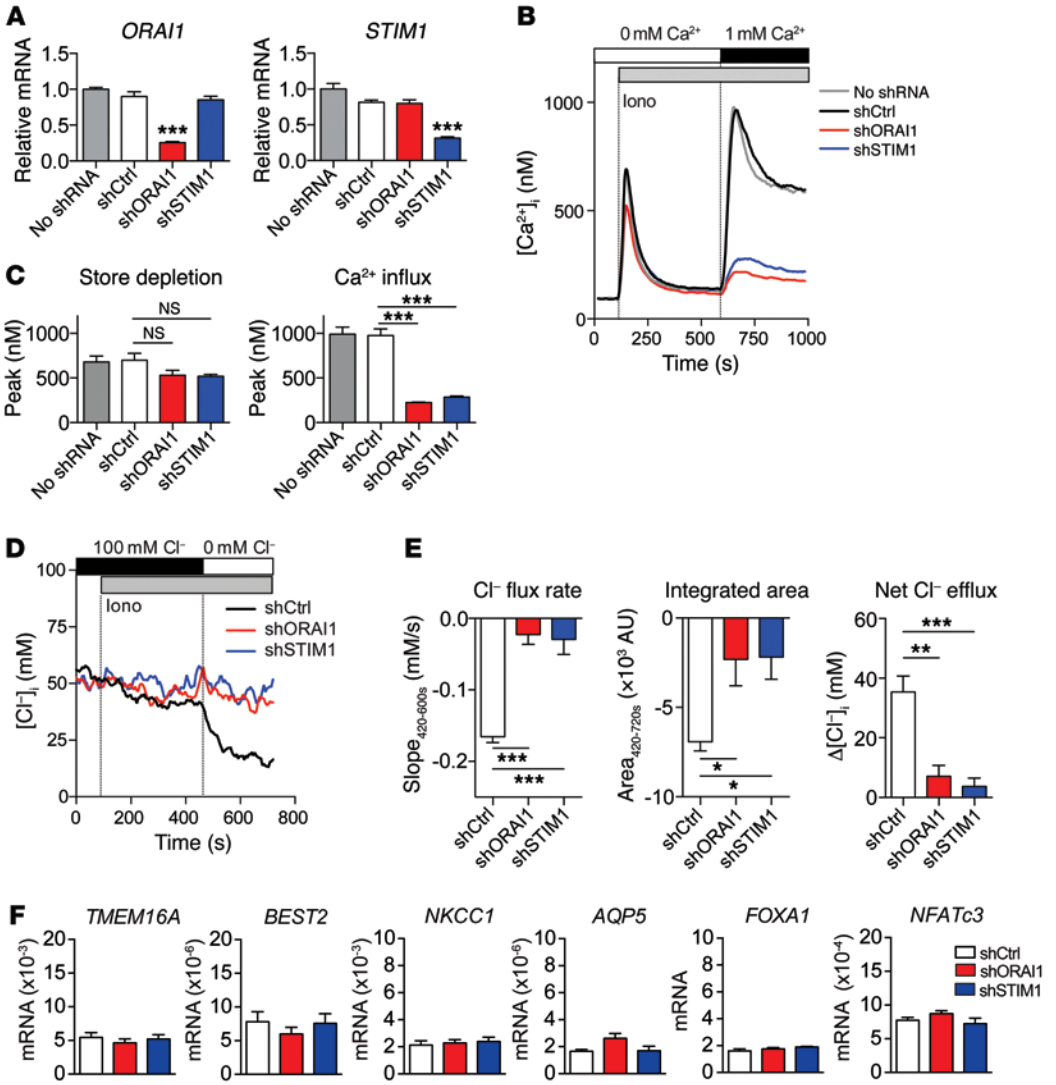

Figure 5. SOCE mediates Cl^- secretion in human sweat gland cells. (**A**–**C**) NCL-SG3 cells were stably transduced with shORAI1, shSTIM1, control shRNA or left untransduced. (**A**) *ORAI1* (left) and *STIM1* (right) mRNA expression measured by quantitative real-time PCR. mRNA expression in shORAI1- and shSTIM1-transduced cells was normalized to that in nontransduced cells (no shRNA). *GAPDH* mRNA was used as a housekeeping control. Shown are the mean ± SEM of 5 independent experiments done in triplicates. (**B**) Representative $[Ca^{2+}]_i$ measurements in NCL-SG3 cells. Fura-2-loaded cells were stimulated with 1 μM ionomicyn (Iono) in Ca^{2+}-free Ringer solution followed by readdition of 1 mM Ca^{2+} to induce SOCE. For additional details see Supplemental Methods. (**C**) Peak of $[Ca^{2+}]_i$ after store depletion (left) and SOCE (right) in NCL-SG3 cells. Data are the mean ± SEM of 6 independent experiments done in duplicates. (**D** and **E**) $[Cl^-]_i$ measurements in MQAE-loaded NCL-SG3 cells. Cells were stimulated with 1 μM ionomycin (Iono) to induce SOCE in buffer containing 100 mM Cl^- followed by removal of extracellular Cl^- to force Cl^- secretion from the cells. (**D**) Averaged $[Cl^-]_i$ traces from 50 cells in 1 experiment, and representative of 5 independent experiments. (**E**) Analysis of Cl^- efflux rates (left), reduction in $[Cl^-]_i$ (middle; calculated as the integrated $area_{420\text{-}720s}$ relative to baseline) and net Cl^- efflux (right) after removal of extracellular Cl^- at 420 seconds as shown in **D**. Net Cl^- efflux was calculated as mean baseline $[Cl^-]_i$ (0–90 seconds) minus mean $[Cl^-]_i$ (500–700 seconds). Data shown are the mean ± SEM of 5 independent experiments. (**F**) mRNA expression of *TMEM16A*, *BEST2*, *NKCC1*, *AQP5*, *FOXA1* and *NFATc3* in shRNA-transduced NCL-SG3 cells analyzed by quantitative real-time PCR. Data shown are the mean ± SEM of 4-5 independent experiments done in triplicates. Statistical analyses in **A**, **C**, and **E** were performed using 1-way ANOVA followed by Bonferroni post hoc test. $^*P < 0.05$, $^{**}P < 0.01$, $^{***}P < 0.001$.

with ORAI1-deficient cells (Figure 6F), consistent with residual Ca^{2+} store depletion but impaired SOCE in the absence of ORAI1 (Figure 5B). CaCC currents in trypsin-stimulated WT NCL-SG3 cells were robust and sustained, whereas those in ORAI1-deficient cells were smaller and more transient (Figure 6, G and H), similar to results obtained after ionomycin stimulation. Taken together, CRAC channel function and SOCE triggered either by passive depletion of Ca^{2+} stores or by agonist stimulation are essential to activate CaCCs and Cl^- secretion.

SOCE mediates Cl^- secretion in human eccrine sweat gland cells by activating TMEM16A. The identity of the CaCCs in eccrine sweat gland cells is controversial (3, 7, 24). In mice, deletion of *Best2* gene expression impairs sweating (24), whereas TMEM16A was suggested to mediate CaCC-dependent Cl^- secretion in human sweat gland cells (7). We found TMEM16A expression in primary human eccrine sweat glands from a healthy donor (Supplemental Figure 6A). Its expression was not altered in CRAC channel–deficient patients with *ORAI1* p.V181SfsX8 null or *STIM1* p.P165Q loss-of-

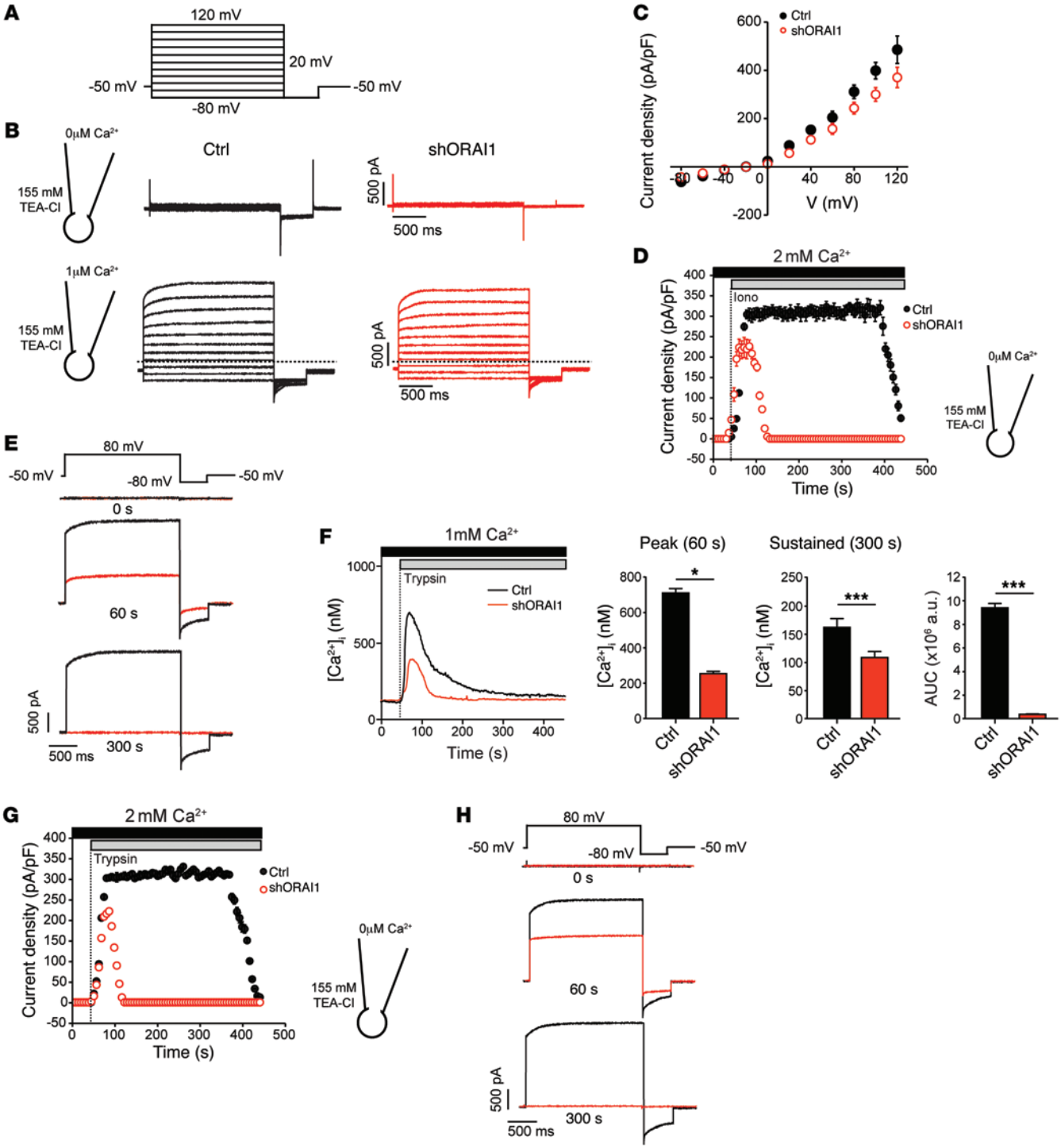

Figure 6. SOCE activates Ca^{2+}-dependent Cl^- channels (CaCCs) in human sweat gland cells. NCL-SG3 cells were transduced with shORAI1 (red) or left untransduced (Ctrl, black) and Cl^- currents measured by whole-cell patch-clamp. (**A**) Currents were elicited by 20-mV steps from –80 mV to 120 mV (from a holding potential of –50 mV) followed by a 0.5-second hyperpolarizing step to –80 mV. (**B**) Representative current traces recorded in individual Ctrl and shORAI1-transduced NCL-SG3 cells with 0 μM Ca^{2+} (top) or 1 μM Ca^{2+} (bottom) present in the patch pipette. Dotted lines indicate the zero-current level. (**C**) Current density as a function of voltage at the end of each test pulse from experiments shown in **B** (mean ± SEM, n = 5 per cell line). The reversal potential of the current is close to the equilibrium potential of Cl^- (E_{Cl} ~ –24 mV). (**D**) Current densities in NCL-SG3 cells stimulated with 1 μM ionomycin (Iono). Currents were elicited by consecutive 2-second voltage steps to 80 mV, followed by a 0.5-second hyperpolarizing step to –80 mV (mean ± SEM, n = 5 cells per cell line). (**E**) Representative Cl^- current traces extracted at 0, 60 and 300 seconds from the experiment in **D**. (**F**) Representative $[Ca^{2+}]_i$ traces from NCL-SG3 cells stimulated with 10 μM trypsin (left) and quantitation of $[Ca^{2+}]_i$ at 60 seconds (peak) and 300 seconds (sustained phase). The AUC was integrated between 50 and 300 seconds (mean ± SEM of 3 independent experiments, n = 15 cells analyzed per experiment). Statistical significance was determined using a 2-tailed Student's t test. $^*P < 0.05$, $^{***}P < 0.001$. (**G**) Current densities were recorded in NCL-SG3 cells stimulated with 10 μM trypsin using an identical pulse protocol to **E**. (mean ± SEM, n = 5). (**H**) Representative Cl^- current traces extracted at 0, 60 and 300 seconds from the experiment shown in **G**. TEA-Cl, tetraethylammonium chloride.

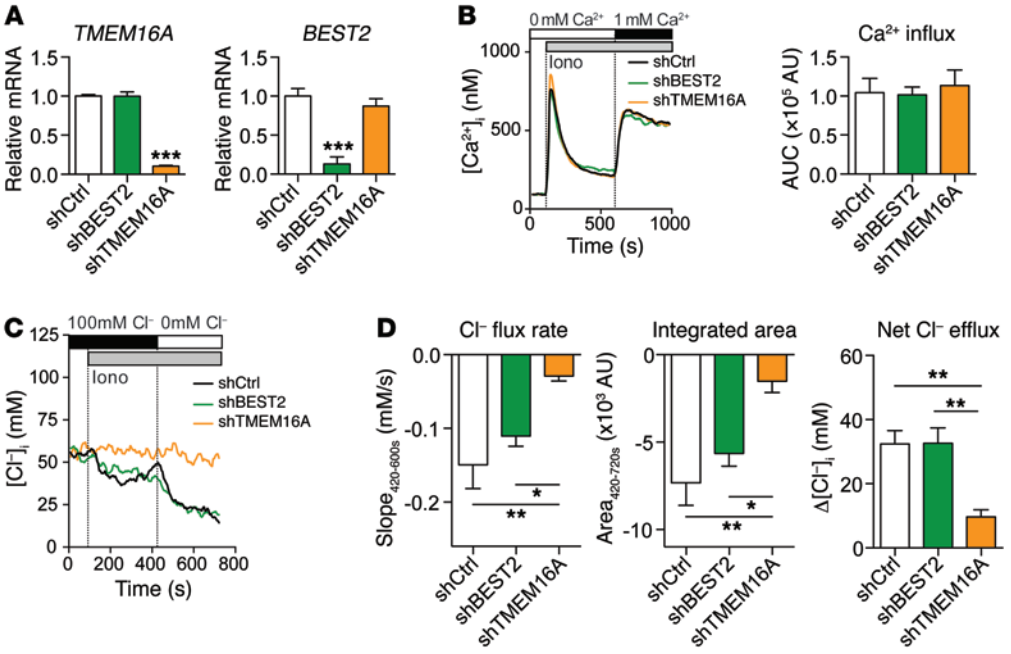

Figure 7. TMEM16A mediates SOCE-induced Cl^- secretion in human sweat gland cells. NCL-SG3 cells were stably transduced with shBEST2, shTMEM16A, or control shRNA (shCtrl). (**A**) *TMEM16A* and *BEST2* mRNA expression measured by quantitative real-time PCR and normalized to levels in shCtrl-transduced cells. *GAPDH* was used as a housekeeping control. Mean ± SEM of 3 independent experiments done in triplicate. (**B**) $[Ca^{2+}]_i$ measurements in Fura-2–loaded NCL-SG3 cells stimulated with 1 μM ionomycin (Iono) in Ca^{2+}-free Ringer solution followed by readdition of 1 mM Ca^{2+} to induce SOCE. Representative $[Ca^{2+}]_i$ traces (left) and AUC (right) after readdition of 1 mM Ca^{2+} (Ca^{2+} influx phase). For additional details see Supplemental Methods. Bar graphs represent mean ± SEM of 3 independent experiments done in triplicate. (**C** and **D**) $[Cl^-]_i$ measurements in MQAE-loaded NCL-SG3 cells analyzed by single-cell time-lapse fluorescence microscopy. Cells were stimulated with 1 μM ionomycin (Iono) to induce SOCE in buffer containing 100 mM Cl^- followed by removal of extracellular Cl^- to force Cl^- secretion. The Ca^{2+} concentration in the extracellular buffer remained constant (1.8 mM) throughout the experiment. (**C**) $[Cl^-]_i$ traces averaged from 50 cells in 1 experiment, and representative of 6–7 independent experiments. (**D**) Analysis of Cl^- efflux rates (420–600 seconds, left), reduction in $[Cl^-]_i$ (middle; calculated as the integrated $area_{420-720s}$ relative to baseline), and net Cl^- efflux (right) after removal of extracellular Cl^- at 420 seconds from data shown in **C**. For additional details see Figure 5E and Supplemental Methods. Data in **D** are mean ± SEM of 7 independent experiments for shCtrl, and 6 for both shBEST2 and shTMEM16A. Statistical analyses in **A** and **D** were performed using 1-way ANOVA followed by Bonferroni post hoc test. $^*P < 0.05$, $^{**}P < 0.01$, $^{***}P < 0.001$.

function mutations (not shown). TMEM16A was also detectable by Western blot in NCL-SG3 cells (Supplemental Figure 6B). To functionally assess which CaCC mediates Cl^- secretion in human eccrine sweat gland cells, we stably deleted *TMEM16A* and *BEST2* expression in NCL-SG3 cells with shRNAs (Figure 7A and Supplemental Figure 6B). Suppression of TMEM16A or BEST2 had no effect on Ca^{2+} influx in NCL-SG3 cells (Figure 7B), indicating that these CaCCs do not regulate the membrane potential that is required for SOCE. Whereas deletion of *BEST2* expression had no effect on Cl^- secretion by NCL-SG3 cells, TMEM16A-deficient NCL-SG3 cells showed abolished Cl^- secretion after ionomycin stimulation and removal of extracellular Cl^- (Figure 7, C and D). These data suggested that TMEM16A, but not BEST2, is activated by SOCE and mediates Cl^- secretion in human sweat gland cells.

We next measured Ca^{2+}-activated Cl^- currents in TMEM16A- and BEST2-deficient NCL-SG3 cells using whole-cell current recordings. In the presence of 1 μM Ca^{2+} in the patch pipette, and thus the cytosol, we observed robust Cl^- currents in shBEST2-transduced cells, which had properties identical to those in untransduced NCL-SG3 cells (Figure 8, A and B, and Figure 6). By contrast, no Cl^- currents or barely detectable Cl^- currents were found in shTMEM16A-transduced cells under the same conditions (Figure 8, A and B), indicating that TMEM16A is the main CaCC in human eccrine sweat gland cells.

It is possible that activation of BEST2, unlike that of TMEM16A, requires additional signals besides Ca^{2+} that are generated by agonist stimulation. To verify that TMEM16A is the physiological CaCC in human eccrine sweat gland cells, we stimulated NCL-SG3 cells with the PAR2 agonist trypsin. Neither deletion of *TMEM16A* nor that of *BEST2* affected Ca^{2+} influx in NCL-SG3 cells after trypsin stimulation (Figure 8C). Trypsin induced strong Cl^- currents in shBEST2-transduced cells (Figure 8, D and E) that had properties similar to those in WT NCL-SG3 cells (Figure 6). By contrast, deletion of *TMEM16A* almost completely abolished the trypsin-induced Cl^- currents in NCL-SG3 cells during both the store-depletion and the SOCE phase of the Ca^{2+} response (Figure 8, D and E). A similar defect in trypsin-induced CaCC currents was detected in shTMEM16A-transduced but not in WT and shBEST2-transduced NCL-SG3 cells when we used a weak Ca^{2+} buffer in the patch pipette (Supplemental Figure 7). The Cl^- current properties were similar to those observed in previous experiments (Figure 8D and Supplemental Figure 7), but the transient current kinetics mimicked more closely those of trypsin-induced SOCE (Figure 8C and Supplemental Figure 7A). It is noteworthy that we observed residual Cl^- currents before trypsin stimulation in WT and shBEST2-transduced NCL-SG3 cells (Supplemental Figure 7, A and B). These results are consistent with the expression of the TMEM16A(*ac*) splicing variant in NCL-SG3 cells (7), which has high affinity for Ca^{2+} and is active at negative membrane potentials (55). Taken together, our results show that SOCE mediated by ORAI1 and STIM1 is essential for Cl^- secretion via the Ca^{2+}-activated Cl^- channel TMEM16A, and thus controls eccrine sweat gland function and thermoregulation.

Discussion

We identified CRAC channels and SOCE as a critical signaling pathway for eccrine sweat gland function in humans and mice.

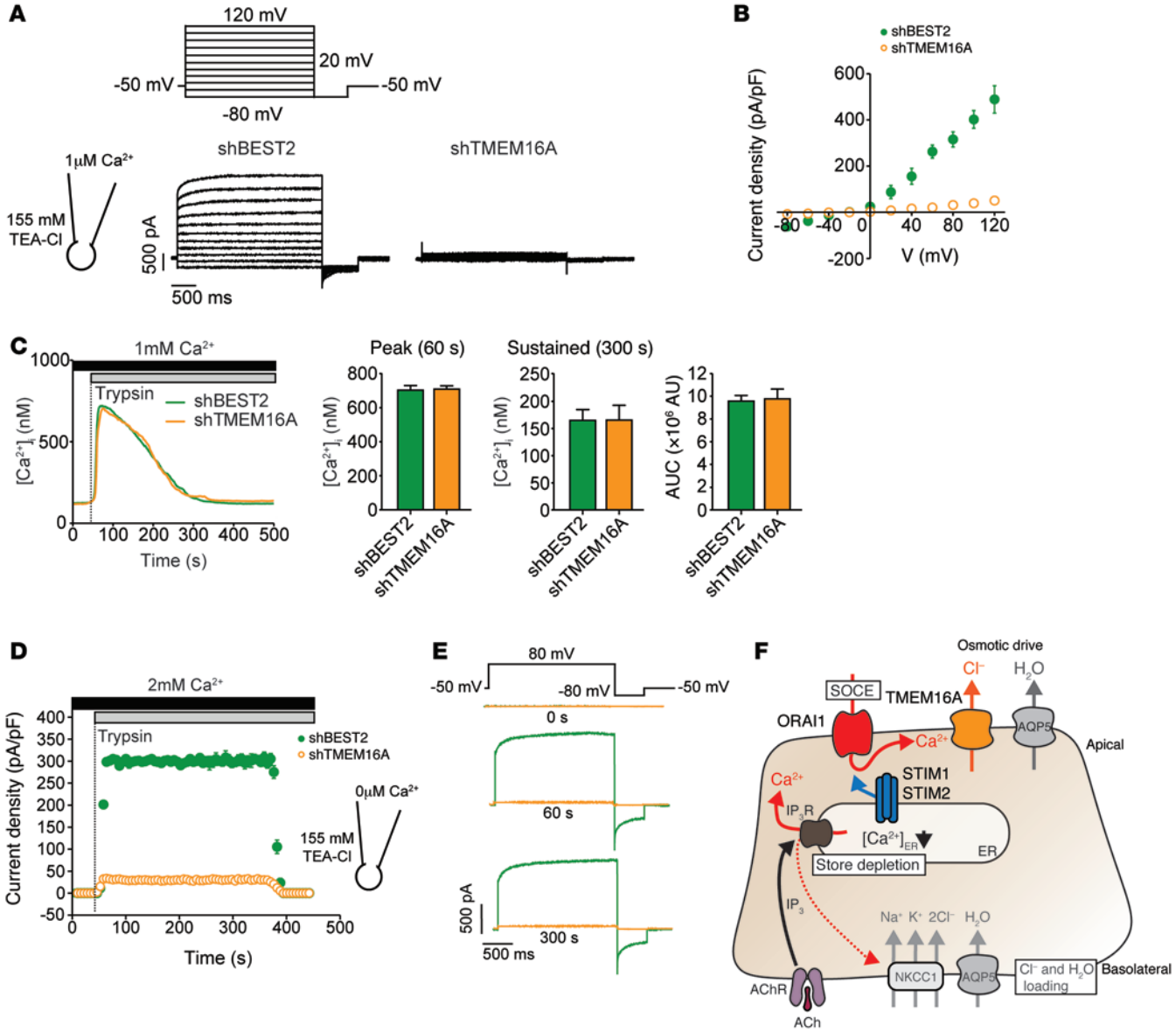

Figure 8. SOCE-induced Cl^- currents in human sweat gland cells are mediated by TMEM16A. (**A**–**E**) NCL-SG3 cells were stably transduced with shBEST2 and shTMEM16A, and analyzed for Cl^- currents by patch clamping in whole-cell configuration. (**A**) Recording protocol (top): Currents were elicited by 20-mV steps from –80 mV to 120 mV (from a holding potential of –50 mV) followed by a 0.5-second hyperpolarizing step to –80 mV. Representative current traces (bottom) recorded in individual shBEST2- and shTMEM16A-transduced NCL-SG3 cells with 1 μM Ca^{2+} present in the patch pipette. (**B**) Current density versus voltage relationships determined at the end of each test pulse from experiments shown in **A**. Data are mean ± SEM of 5 cells for shBEST2 and 8 cells for shTMEM16A. (**C**) Ca^{2+} influx in shRNA-transduced NCL-SG3 cells following agonist stimulation was measured and analyzed as described in Figure 6F. Representative $[Ca^{2+}]_i$ traces from 1 experiment (left) and quantitation of peak $[Ca^{2+}]_i$ at 60 seconds and 300 seconds, and the overall $[Ca^{2+}]_i$ increase (AUC) from 50–300 seconds. Data are mean ± SEM of 4 independent experiments with at least 10 cells analyzed per experiment. (**D**) Current densities in NCL-SG3 cells stimulated with 10 μM trypsin in 2 mM Ca^{2+}-containing extracellular buffer. Currents were elicited by consecutive 2-second voltage steps to 80 mV, followed by a 0.5-second hyperpolarizing step to –80 mV. Data are mean ± SEM of 8 cells for shBEST2 and 11 cells for shTMEM16A. (**E**) Representative Cl^- current traces from individual shBEST2- and shTMEM16A-transduced NCL-SG3 cells extracted at 0 seconds, 60 seconds, and 300 seconds from the experiment shown in **D**. (**F**) Schematic representation of SOCE-induced TMEM16A activation and Cl^- secretion. AChR stimulation results in IP_3-mediated release of Ca^{2+} from ER stores, which activates STIM1 and STIM2, allowing them to bind to and open the store-operated CRAC channel ORAI1. SOCE via ORAI1 activates TMEM16A Cl^- channels and Cl^- secretion, which provides the osmotic driving force for water flow and sweat production. For details see text. TEA-Cl, tetraethylammonium chloride.

CRAC channels were required to activate Ca^{2+}-activated Cl^- channels, in particular TMEM16A, and to induce Cl^- secretion. This pathway is disrupted in human patients with CRAC channelopathy due to null or loss-of-function mutations in the *ORAI1* and *STIM1* genes. Their disease is characterized by EDA as well as severe immunodeficiency, skeletal myopathy, and hypocalcified dental enamel (29, 30). The patients' anhidrosis presents clinically with hyperthermia especially in hot summer months and was reported in most, but not all, ORAI1- or STIM1-deficient patients. However, all patients in whom sweating was tested directly by pilocarpine iontophoresis uniformly lacked sweat production (35, 38, 41, 43). In those CRAC channel–deficient patients in whom

anhidrosis was not reported, it may have gone unnoticed because of a focus on their severe immunodeficiency disease and early death (35–37, 39, 41, 42). Alternatively, several patients with hypomorphic *ORAI1* mutations and reduced but not abolished SOCE may have hypohidrosis that is more difficult to diagnose (40, 42). Skin biopsies of patients with *ORAI1* and *STIM1* mutations show eccrine sweat glands with morphologies and cellular compositions similar to those of healthy donors but significantly reduced lumen of the sweat acini, which is consistent with similar findings in $Orai1^{K14Cre}$ and $Stim1/2^{K14Cre}$ mice. CRAC channels and SOCE therefore do not appear to be required for the development of eccrine sweat glands, but instead control their secretory function. This is in contrast to patients with EDA-ID resulting from mutations in *IKBKG* and *NFKBIA* (OMIM #300291) (32–34, 57, 58), who have abnormal development of ectoderm-derived tissues including the skin, hair, teeth, and eccrine sweat glands. Thus, mutations of genes in the NF-κB signaling pathway (*IKBKG*, *NFKBIA*) and in the CRAC channel complex (*ORAI1*, *STIM1*) both cause EDA-ID, but the underlying causes of anhidrosis are different. Whereas the NF-κB pathway controls the development of sweat glands, CRAC channels regulate sweat gland function via the activation of CaCCs.

Ca^{2+} signals control the transcriptional regulation of gene expression in many cell types (59). It was therefore possible that CRAC channel deficiency interferes with eccrine sweat gland function by altering the expression of ion channels or transporters. However, we did not find evidence that SOCE is required for the expression of molecules involved in sweat production such as TMEM16A, BEST2, NKCC1, and AQP5 (3–5, 7, 24, 49). The 2 main CaCCs that have been implicated in sweat gland function, TMEM16A and BEST2, were expressed normally at transcript and protein levels in murine and human sweat gland cells that lack SOCE. Further supporting the role of SOCE in regulating the function but not the expression of Cl^- channels involved in sweat secretion was our finding that acute inhibition of SOCE in the paws of mice with the CRAC channel inhibitor BTP2 significantly reduced ACh-stimulated sweat secretion. A direct Ca^{2+}-dependent regulation of CaCCs is also consistent with the fact that addition of 1 μM Ca^{2+} inside the patch pipette was sufficient for the activation of Cl^- currents even in the absence of ORAI1 expression.

CaCCs have long been recognized to be important for sweat gland function (7, 17), and Cl^- secretion in the human eccrine sweat gland cell line NCL-SG3 was shown to depend on increases in $[Ca^{2+}]_i$ (7, 15, 17). However, the source of Ca^{2+} to activate CaCCs remains debated. Recently, patients with missense mutations in the *ITPR2* gene encoding IP_3R2 were reported to suffer from a generalized, isolated hypohidrosis without other symptoms characteristic of EDA such as skin, hair, or tooth defects (16). IP_3R2 is 1 of 3 IP_3R homologs that are localized in the ER membrane and function as nonselective Ca^{2+} release channels whose opening results in a transient $[Ca^{2+}]_i$ increase. Sweat gland cells from $Itpr2^{-/-}$ mice had reduced ACh-induced Ca^{2+} signals, and $Itpr2^{-/-}$ mice showed impaired sweat secretion in response to cholinergic stimulation (16). It was therefore concluded that Ca^{2+} released from the ER via IP_3R2 controls sweat gland function. This is intriguing because IP_3Rs were shown to colocalize with CaCCs required for Cl^- secretion in several cell types (60–62). However, Ca^{2+} release from the ER via IP_3R2 not only increases $[Ca^{2+}]_i$ and may thus contribute to CaCC activation but also decreases $[Ca^{2+}]_{ER}$, which is the trigger for the activation of STIM1 and STIM2 and the opening of store-operated CRAC channels. Thus, mutations or deletion of IP_3R2 that inhibit Ca^{2+} release from the ER will also impair the activation of SOCE. Our data support the notion that the hypohidrosis observed in patients with IP_3R2 mutation is due to defective CRAC channel activation and furthermore that SOCE is essential for sweat gland function whereas Ca^{2+} released from the ER is not sufficient. This conclusion is based on the fact that the release of Ca^{2+} from intracellular stores is intact in (i) primary sweat gland cells isolated from $Orai1^{K14Cre}$ and $Stim1/2^{K14Cre}$ mice, (ii) NCL-SG3 cells transduced with shRNAs against STIM1 or ORAI1, and (iii) cells from patients with loss-of-function mutations in *ORAI1* or *STIM1* genes (35, 38, 44, 63). This conclusion is further supported by the fact that the transient Ca^{2+} signals in ORAI1-deficient NCL-SG3 cells after ionomycin or trypsin stimulation, which are due to Ca^{2+} release from ER stores, are not sufficient for sustained activation of Cl^- currents and Cl^- secretion. The hypohidrotic phenotype in IP_3R2 mutant patients is fully consistent with a critical role of SOCE in eccrine sweat gland function because of the role of IP_3R2 as an ER leak channel upstream of CRAC channel activation. Interestingly, a recent study proposed a model of how CRAC channels and IP_3Rs may work in tandem to regulate the Ca^{2+}-dependent activation of CaCCs (64). Based on studies in *Xenopus* oocytes, Ca^{2+} entering the cytosol through CRAC channels is taken up by the ER via sarco/endoplasmic Ca^{2+} ATPase (SERCA) pumps and released at different sites by IP_3Rs to activate CaCCs. In this model, IP_3Rs but not CRAC channels colocalize with CaCCs. Whether a similar mechanism plays a role in eccrine sweat gland cells remains to be investigated.

Not only the source of Ca^{2+} for CaCC activation but also the molecular nature of CaCCs themselves in eccrine sweat glands is debated. The most likely candidates are TMEM16A and BEST2. TMEM16A has been proposed to be the prototypical CaCC responsible for Ca^{2+}-dependent Cl^- secretion in several epithelia (20, 65, 66). TMEM16A was found to be strongly expressed in the apical membrane of mouse salivary gland acinar cells (18, 20, 23), and conditional deletion of *Tmem16a* abolished cholinergic-induced fluid secretion (18). Moreover, $Tmem16a^{-/-}$ mice had impaired Ca^{2+}-activated Cl^- secretion in airway and colon epithelia, and pancreatic acinar cells (21). Recent findings in NCL-SG3 cells and isolated human eccrine sweat gland cells from biopsy samples showed mRNA expression of several splice variants of *TMEM16A* (7). Nevertheless, evidence for TMEM16A protein expression in primary human and mouse eccrine sweat glands has been missing. We found that TMEM16A protein is strongly expressed in the apical membrane of murine eccrine sweat glands, consistent with its potential role as a CaCC. In human eccrine sweat glands, TMEM16A localization was not restricted to the apical membrane but was found to be more homogenously distributed in cells, which may have to do with the different placement of clear and dark cells in mouse and human eccrine sweat glands (1, 45, 49). The Cl^- currents we recorded in NCL-SG3 cells closely resembled those reported for TMEM16A, in particular the TMEM16A(*ac*) splice variant, which displays larger instantaneous current and smaller time-dependent activation at positive membrane potential and higher Ca^{2+} sensitivity compared with other splice variants (55)

and which has been reported to be expressed in NCL-SG3 cells (7). Most importantly, deletion of *TMEM16A* in NCL-SG3 sweat gland cells abolished Cl^- secretion and Cl^- currents activated by either Ca^{2+} in the patch pipette or the PAR2 agonist trypsin. These data demonstrate that TMEM16A is essential for CaCC function and Cl^- secretion in human eccrine sweat gland cells and that its activation depends on SOCE.

BEST2 belongs to a small family of anion channels (BEST1–4), which have been linked to bicarbonate transport in intestinal epithelial cells (67), regulation of voltage-dependent Ca^{2+} channels (68), and Cl^- transport in the ER (60). A role for BEST2 in sweat secretion is supported by the lack of spontaneous sweating in *Best2*$^{-/-}$ mice (24), although it is noteworthy that *Best2*$^{-/-}$ mice were not tested for agonist-induced sweating, and it is possible that they have residual sweat production in response to cholinergic stimulation, which might point to an additional role of other CaCCs such as TMEM16A in Cl^- secretion by sweat gland cells in mice. We found BEST2 protein to be expressed in murine eccrine sweat glands, although it was localized predominantly in the cytoplasm, similar to published observations (24). It has been reported that BEST2 is not expressed by all mouse sweat gland secretory cells but only in dark cells (24) that support sweat secretion by clear cells (3). In human NCL-SG3 cells, shRNA-mediated deletion of *BEST2* had no effect on Cl^- secretion or Cl^- currents activated by Ca^{2+} in the patch pipette or trypsin stimulation, suggesting that BEST2 does not contribute to SOCE-induced Cl^- secretion in these cells. Compared with TMEM16A, mRNA expression of *BEST2* in NCL-SG3 cells was much lower, potentially explaining its negligible role.

In addition to controlling CaCC function and Cl^- secretion, SOCE may regulate additional processes involved in sweating. For instance, Ca^{2+} signals in epithelial cells were shown to mediate the translocation of the water channel AQP5 to the apical membrane of salivary (69) and sweat gland cells (70). AQP5 has been proposed to be the main channel mediating water transport in eccrine sweat glands (5, 49, 70). However, despite consensus about the localization of AQP5 in the apical membrane of the mouse sweat gland cells (5, 71), *Aqp5*$^{-/-}$ mice produced ambiguous results, as they had either normal (71) or impaired (5) sweat production. Another potential role for SOCE in eccrine sweat glands is the regulation of myoepithelial cell contraction. Myoepithelial cells are smooth muscle cells found in exocrine glands such as sweat, salivary, lacrimal, and mammary glands. In sweat glands, myoepithelial cells surround the secretory coil, and their contraction has been suggested to facilitate sweat secretion in response to ACh (72). Lack of SOCE in *Orai1*$^{-/-}$ mice abolishes lactation due to impaired milk ejection from mammary gland secretory alveoli, which in turn was caused by decreased myoepithelial cell contraction (73). The role of SOCE in sweat gland myoepithelial cell function remains to be elucidated. While defects in AQP5 trafficking to the PM or myoepithelial cell contraction may potentially contribute to anhidrosis in CRAC channel–deficient patients and mice, we show in this study that sweat production already fails at an earlier step because of impaired SOCE-dependent CaCC function and Cl^- secretion.

In summary, we identify CRAC channels and SOCE as an essential pathway required for sweating and thermoregulation. Whereas ORAI1 and STIM1 do not appear to be required for sweat gland development, their function is critical for the activation of CaCCs and Cl^- secretion. We identify TMEM16A as the SOCE-activated CaCC responsible for Cl^- secretion in human eccrine sweat gland cells. Our data demonstrate that Ca^{2+} influx through store-operated CRAC channels is the source of Ca^{2+} required for CaCC activation, Cl^- secretion, and sweat gland function and thus reveal the molecular mechanisms underlying the anhidrosis in patients with loss-of-function mutations in *ORAI1* and *STIM1*. CRAC channelopathy represents a new form of EDA-ID that is due not to an absence of sweat glands but to their impaired function. Besides sweat gland cells, the function of other secretory cells may be regulated by SOCE-dependent activation of CaCCs and Cl^- secretion. Our findings add to the existing evidence supporting an important physiological role of SOCE in regulating the function of exocrine cells including those in the salivary (74), lacrimal (75), and mammary glands (73). From a translational perspective, topical CRAC channel inhibition may be a therapeutic approach for clinical conditions associated with excessive sweating like hyperhidrosis.

Methods

Human samples. Skin biopsies of patients with CRAC channelopathy who are homozygous for *ORAI1* p.R91W (35, 44), *ORAI1* p.V181SfsX8, and *STIM1* p.P165Q (41) mutations and healthy donors were used for histology and immunohistochemistry.

NCL-SG3 cells and shRNA transduction. The human eccrine sweat gland cell line NCL-SG3 was a gift of Roland Lang (Paracelsus Medical University Salzburg, Salzburg, Austria). NCL-SG3 cells were established by infection of primary human secretory eccrine sweat glands with simian virus 40 (SV40) (51). For knockdown of ORAI1, STIM1, BEST2, and TMEM16A expression, NCL-SG3 cells were stably transduced with lentiviral particles expressing ORAI1-, STIM1-, BEST2-, or TMEM16A-specific shRNAs (Supplemental Table 1). The knockdown efficiency was evaluated by quantitative real-time PCR, flow cytometry (ORAI1), and Western blotting (STIM1 and TMEM16A). Two to three shRNAs per gene were tested, and those with the best knockdown efficiency were used for experiments. Additional details regarding cell culture, transduction of NCL-SG3 cells, flow cytometry, and Western blotting can be found in Supplemental Methods.

Mice. *Orai1*$^{fl/fl}$ (76) and *Stim1*$^{fl/fl}$ *Stim2*$^{fl/fl}$ mice (77) have been described previously. They were crossed to *K14-Cre* mice (78) (The Jackson Laboratory, strain 004782) to generate *Orai1*$^{fl/fl}$ *K14-Cre* (*Orai1*^{K14Cre}) and *Stim1*$^{fl/fl}$ *Stim2*$^{fl/fl}$ *K14-Cre* (*Stim1/2*^{K14Cre}) mice. *Orai2*$^{-/-}$ mice were generated using VGB6 ES cells (C57BL/6NTac) obtained from the Knockout Mouse Project (KOMP, www.komp.org) repository at UC Davis (project ID VG14962, Orai2tm1(KOMP)Vlcg).

All mice were maintained on a C57BL/6 genetic background and used between 6 and 16 weeks of age.

Sweat testing. Sweat secretion in mice was measured using the iodine-starch sweat test as previously described (46). Additional details can be found in Supplemental Methods.

Histology, immunohistochemistry, immunofluorescence, and image analysis. Details regarding sample processing, histology, immunohistochemistry, immunofluorescence, and image analysis are described in Supplemental Methods.

Sweat gland isolation from mice. Tips of mouse digits were dissected with micro-scissors and fine-tip forceps under a stereoscope microscope, and pieces of skin tissue were digested with 0.25 mg/ml Liber-

ase TM (Roche) in DMEM (Corning) for 45 minutes at 37°C. Digested tissue was passed through a 40-μm cell strainer (Fisher Scientific), and gland tissue retained in the filter was collected for quantitative real-time PCR analysis and intracellular Ca^{2+} and Cl^- measurements.

Measurement of intracellular Ca^{2+} levels in isolated sweat glands and cell lines. Measurements of intracellular Ca^{2+} levels were performed as described previously (63). Additional details can be found in Supplemental Methods.

Measurement of intracellular Cl^- levels in isolated sweat glands and cell lines. $[Cl^-]_i$ was measured using the MQAE [*N*-(ethoxycarbonylmethyl)-6-methoxyquinolinium bromide] dye as described (79). Additional details regarding $[Cl^-]_i$ measurements can be found in Supplemental Methods.

Real-time PCR. Total RNA from freshly isolated mouse sweat glands and NCL-SG3 cell lines was extracted with TRIzol (Invitrogen), reverse transcribed using the iScript cDNA synthesis kit (Bio-Rad), and analyzed by quantitative real-time PCR using Maxima SYBR Green qPCR Master Mix (Thermo Fisher Scientific) and gene-specific primers (Supplemental Table 2). Values of mRNA expression were normalized to the human *GAPDH* or the mouse hypoxanthine guanine phosphoribosyl transferase (*Hprt*) housekeeping gene, respectively, using the $2^{-\Delta\Delta CT}$ method.

Patch clamp electrophysiology. For measurements of Cl^- currents, NCL-SG3 cells were grown on glass coverslips for 1–3 days before experimentation. Coverslips were transferred to a chamber containing extracellular bath solution (155 mM tetraethylammonium chloride to block K^+ channels, 2 mM $CaCl_2$, 1 mM $MgCl_2$, 10 mM HEPES, pH 7.2). Cl^- currents in individual cells were measured in the whole-cell patch clamp configuration using pClamp 9 and an Axopatch 200B amplifier (Molecular Devices). Recordings were sampled at 2 kHz and filtered at 1 kHz. Pipette resistances were 3–5 megaohms, and seal resistances were greater than 1 gigaohm. Pipette solutions (pH 7.2) contained 60 mM tetraethylammonium chloride, 90 mM tetraethylammonium glutamate, 10 mM HEPES, and either 1 mM EGTA without added Ca^{2+} to yield negligible free Ca^{2+} or 5 mM EGTA with 4.3 mM $CaCl_2$ added to yield 1 μM free Ca^{2+}. Alternatively, 1 mM HEDTA (*N*-(2-hydroxyethyl)ethylenediamine-*N,N',N'*-triacetic acid) and 20 μM $CaCl_2$ were used in the internal pipette solution to better mimic physiological buffering and basal $[Ca^{2+}]_i$ conditions (~100 nM Ca^{2+}). Free $[Ca^{2+}]$ was estimated using Maxchelator freeware (http://maxchelator.stanford.edu/). Agonists were directly perfused onto individual cells using a multibarrel perfusion pipette.

Statistics. Data are expressed as mean ± SEM. Normally distributed variables according to the Kolmogorov-Smirnov or the Shapiro-Wilk test were analyzed by 2-tailed Student's *t* test for comparisons between 2 groups and 1-way ANOVA and Bonferroni post hoc test for comparisons between more than 2 groups. Statistical analyses were performed using GraphPad Prism 6 software. A value of *P* less than 0.05 was considered statistically significant.

Study approval. All animal procedures were conducted in accordance with a protocol approved by the Institutional Animal Care and Use Committee of New York University Langone Medical Center. For experiments using human tissue, informed consent for the studies was obtained from the patients' families in accordance with the Declaration of Helsinki and Institutional Review Board approval of the New York University School of Medicine.

Author contributions

ARC, DIY, and SF designed the research; ARC, MV, LEW, ME, LH, JY, HPS, and CW performed experiments; MS, SC, SET, TI, IM, MC, and SF collected samples and obtained clinical data; ARC, MV, LEW, HPS, DIY, and SF analyzed data; DC and RSL contributed reagents; and ARC and SF wrote the paper.

Acknowledgments

This work was funded by NIH grants AI097302 to SF, DE014756 and DE019245 to DIY, and DE022799 to RSL, postdoctoral fellowships from the Alfonso Martin Escudero Foundation (to ARC), and VA 882/1-1 by the Deutsche Forschungsgemeinschaft to MV. The New York University School of Medicine core facility for histopathology is supported in part by NIH grant UL1 TR00038 from the National Center for Advancing Translational Sciences. We thank W. Coetzee (New York University School of Medicine) for critical reading of the manuscript and members of the Feske laboratory for helpful discussions.

Address correspondence to: Stefan Feske, Department of Pathology, New York University School of Medicine, 550 First Avenue, Smilow 316, New York, New York 10016, USA. Phone: 212.263.9066; E-mail: feskes01@nyumc.org

1. Lu C, Fuchs E. Sweat gland progenitors in development, homeostasis, and wound repair. *Cold Spring Harb Perspect Med*. 2014;4(2):a015222.
2. Sato K, Kang WH, Saga K, Sato KT. Biology of sweat glands and their disorders. I. Normal sweat gland function. *J Am Acad Dermatol*. 1989;20(4):537–563.
3. Cui CY, Schlessinger D. Eccrine sweat gland development and sweat secretion. *Exp Dermatol*. 2015;24(9):644–650.
4. Wilson TE, Metzler-Wilson K. Sweating chloride bullets: understanding the role of calcium in eccrine sweat glands and possible implications for hyperhidrosis. *Exp Dermatol*. 2015;24(3):177–178.
5. Nejsum LN, et al. Functional requirement of aquaporin-5 in plasma membranes of sweat glands. *Proc Natl Acad Sci U S A*. 2002;99(1):511–516.
6. Saga K. Structure and function of human sweat glands studied with histochemistry and cytochemistry. *Prog Histochem Cytochem*. 2002;37(4):323–386.
7. Ertongur-Fauth T, Hochheimer A, Buescher JM, Rapprich S, Krohn M. A novel TMEM16A splice variant lacking the dimerization domain contributes to calcium-activated chloride secretion in human sweat gland epithelial cells. *Exp Dermatol*. 2014;23(11):825–831.
8. Torres NE, Zollman PJ, Low PA. Characterization of muscarinic receptor subtype of rat eccrine sweat gland by autoradiography. *Brain Res*. 1991;550(1):129–132.
9. Shibasaki M, Wilson TE, Crandall CG. Neural control and mechanisms of eccrine sweating during heat stress and exercise. *J Appl Physiol*. 2006;100(5):1692–1701.
10. Courtois G, Smahi A. NF-kappaB-related genetic diseases. *Cell Death Differ*. 2006;13(5):843–851.
11. Sadier A, Viriot L, Pantalacci S, Laudet V. The ectodysplasin pathway: from diseases to adaptations. *Trends Genet*. 2014;30(1):24–31.
12. Ray S, Sharma S, Maheshwari A, Aneja S, Kumar A. Heat stroke in an infant with hypohidrotic ectodermal dysplasia: brain magnetic resonance imaging findings. *J Child Neurol*. 2013;28(4):538–540.
13. Cheshire WP. Thermoregulatory disorders and illness related to heat and cold stress. *Auton Neurosci*. 2016;196:91–104.
14. Sato K, Sato F. Role of calcium in cholinergic and adrenergic mechanisms of eccrine sweat secretion. *Am J Physiol*. 1981;241(3):C113–C120.
15. Ring A, Mörk AC, Roomans GM. Calcium-activated chloride fluxes in cultured NCL-SG3 sweat gland cells. *Cell Biol Int*. 1995;19(4):265–278.
16. Klar J, et al. Abolished InsP3R2 function inhibits sweat secretion in both humans and mice. *J Clin*

Invest. 2014;124(11):4773–4780.
17. Servetnyk Z, Roomans GM. Chloride transport in NCL-SG3 sweat gland cells: channels involved. *Exp Mol Pathol*. 2007;83(1):47–53.
18. Catalán MA, et al. A fluid secretion pathway unmasked by acinar-specific Tmem16A gene ablation in the adult mouse salivary gland. *Proc Natl Acad Sci U S A*. 2015;112(7):2263–2268.
19. Nakamoto T, et al. Functional and molecular characterization of the fluid secretion mechanism in human parotid acinar cells. *Am J Physiol Regul Integr Comp Physiol*. 2007;292(6):R2380–R2390.
20. Yang YD, et al. TMEM16A confers receptor-activated calcium-dependent chloride conductance. *Nature*. 2008;455(7217):1210–1215.
21. Ousingsawat J, Martins JR, Schreiber R, Rock JR, Harfe BD, Kunzelmann K. Loss of TMEM16A causes a defect in epithelial Ca^{2+}-dependent chloride transport. *J Biol Chem*. 2009;284(42):28698–28703.
22. Rock JR, et al. Transmembrane protein 16A (TMEM16A) is a Ca^{2+}-regulated Cl^- secretory channel in mouse airways. *J Biol Chem*. 2009;284(22):14875–14880.
23. Romanenko VG, et al. Tmem16A encodes the Ca^{2+}-activated Cl^- channel in mouse submandibular salivary gland acinar cells. *J Biol Chem*. 2010;285(17):12990–13001.
24. Cui CY, et al. Forkhead transcription factor FoxA1 regulates sweat secretion through Bestrophin 2 anion channel and Na-K-Cl cotransporter 1. *Proc Natl Acad Sci U S A*. 2012;109(4):1199–1203.
25. Metzler-Wilson K, et al. Extracellular calcium chelation and attenuation of calcium entry decrease in vivo cholinergic-induced eccrine sweating sensitivity in humans. *Exp Physiol*. 2014;99(2):393–402.
26. Prakriya M, Lewis RS. Store-operated calcium channels. *Physiol Rev*. 2015;95(4):1383–1436.
27. Alzayady KJ, Wang L, Chandrasekhar R, Wagner LE, Van Petegem F, Yule DI. Defining the stoichiometry of inositol 1,4,5-trisphosphate binding required to initiate Ca^{2+} release. *Sci Signal*. 2016;9(422):ra35.
28. Shaw PJ, Qu B, Hoth M, Feske S. Molecular regulation of CRAC channels and their role in lymphocyte function. *Cell Mol Life Sci*. 2013;70(15):2637–2656.
29. Feske S. CRAC channelopathies. *Pflugers Arch*. 2010;460(2):417–435.
30. Lacruz RS, Feske S. Diseases caused by mutations in ORAI1 and STIM1. *Ann N Y Acad Sci*. 2015;1356:45–79.
31. Feske S, Wulff H, Skolnik EY. Ion channels in innate and adaptive immunity. *Annu Rev Immunol*. 2015;33:291–353.
32. Courtois G, et al. A hypermorphic IκBα mutation is associated with autosomal dominant anhidrotic ectodermal dysplasia and T cell immunodeficiency. *J Clin Invest*. 2003;112(7):1108–1115.
33. Döffinger R, et al. X-linked anhidrotic ectodermal dysplasia with immunodeficiency is caused by impaired NF-κB signaling. *Nat Genet*. 2001;27(3):277–285.
34. Fusco F, et al. EDA-ID and IP, two faces of the same coin: how the same IKBKG/NEMO mutation affecting the NF-κB pathway can cause immunodeficiency and/or inflammation. *Int Rev Immunol*. 2015;34(6):445–459.
35. McCarl CA, et al. ORAI1 deficiency and lack of store-operated Ca^{2+} entry cause immunodeficiency, myopathy, and ectodermal dysplasia. *J Allergy Clin Immunol*. 2009;124(6):1311–1318.e7.
36. Picard C, et al. STIM1 mutation associated with a syndrome of immunodeficiency and autoimmunity. *N Engl J Med*. 2009;360(19):1971–1980.
37. Byun M, et al. Whole-exome sequencing-based discovery of STIM1 deficiency in a child with fatal classic Kaposi sarcoma. *J Exp Med*. 2010;207(11):2307–2312.
38. Fuchs S, et al. Antiviral and regulatory T cell immunity in a patient with stromal interaction molecule 1 deficiency. *J Immunol*. 2012;188(3):1523–1533.
39. Wang S, et al. STIM1 and SLC24A4 are critical for enamel maturation. *J Dent Res*. 2014; 93(7 suppl):94S–100S.
40. Chou J, et al. A novel mutation in ORAI1 presenting with combined immunodeficiency and residual T-cell function. *J Allergy Clin Immunol*. 2015;136(2):479–482.e1.
41. Schaballie H, et al. A novel hypomorphic mutation in STIM1 results in a late-onset immunodeficiency. *J Allergy Clin Immunol*. 2015;136(3):816–819.e4.
42. Badran YR, et al. Combined immunodeficiency due to a homozygous mutation in ORAI1 that deletes the C-terminus that interacts with STIM 1. *Clin Immunol*. 2016;166–167:100–102.
43. Parry DA, et al. A homozygous STIM1 mutation impairs store-operated calcium entry and natural killer cell effector function without clinical immunodeficiency. *J Allergy Clin Immunol*. 2016;137(3):955–957.e8.
44. Feske S, et al. A mutation in Orai1 causes immune deficiency by abrogating CRAC channel function. *Nature*. 2006;441(7090):179–185.
45. Munger BL. The ultrastructure and histophysiology of human eccrine sweat glands. *J Biophys Biochem Cytol*. 1961;11:385–402.
46. Srivastava AK, et al. Ectodysplasin-A1 is sufficient to rescue both hair growth and sweat glands in Tabby mice. *Hum Mol Genet*. 2001;10(26):2973–2981.
47. Kennedy WR, Sakuta M, Quick DC. Rodent eccrine sweat glands: a case of multiple efferent innervation. *Neuroscience*. 1984;11(3):741–749.
48. Nejsum LN, Praetorius J, Nielsen S. NKCC1 and NHE1 are abundantly expressed in the basolateral plasma membrane of secretory coil cells in rat, mouse, and human sweat glands. *Am J Physiol, Cell Physiol*. 2005;289(2):C333–C340.
49. Zhang M, et al. Localization of Na(+)-K(+)-ATPase α/β, Na(+)-K(+)-2Cl-cotransporter 1 and aquaporin-5 in human eccrine sweat glands. *Acta Histochem*. 2014;116(8):1374–1381.
50. Davé V, et al. Calcineurin/Nfat signaling is required for perinatal lung maturation and function. *J Clin Invest*. 2006;116(10):2597–2609.
51. Lee CM, Dessi J. NCL-SG3: a human eccrine sweat gland cell line that retains the capacity for transepithelial ion transport. *J Cell Sci*. 1989;92(pt 2):241–249.
52. Bovell DL, et al. Galanin is a modulator of eccrine sweat gland secretion. *Exp Dermatol*. 2013;22(2):141–143.
53. Mörk AC, von Euler A, Roomans GM, Ring A. cAMP-induced chloride transport in NCL-SG3 sweat gland cells. *Acta Physiol Scand*. 1996;157(1):21–32.
54. Wilson SM, et al. The regulation of membrane 125I- and 86Rb+ permeability in a virally transformed cell line (NCL-SG3) derived from the human sweat gland epithelium. *Exp Physiol*. 1994;79(3):445–459.
55. Ferrera L, et al. Regulation of TMEM16A chloride channel properties by alternative splicing. *J Biol Chem*. 2009;284(48):33360–33368.
56. Bovell DL, et al. Activation of chloride secretion via proteinase-activated receptor 2 in a human eccrine sweat gland cell line — NCL-SG3. *Exp Dermatol*. 2008;17(6):505–511.
57. Jain A, Ma CA, Liu S, Brown M, Cohen J, Strober W. Specific missense mutations in NEMO result in hyper-IgM syndrome with hypohydrotic ectodermal dysplasia. *Nat Immunol*. 2001;2(3):223–228.
58. Zonana J, et al. A novel X-linked disorder of immune deficiency and hypohidrotic ectodermal dysplasia is allelic to incontinentia pigmenti and due to mutations in IKK-γ (NEMO). *Am J Hum Genet*. 2000;67(6):1555–1562.
59. Clapham DE. Calcium signaling. *Cell*. 1995;80(2):259–268.
60. Barro-Soria R, Aldehni F, Almaça J, Witzgall R, Schreiber R, Kunzelmann K. ER-localized bestrophin 1 activates Ca^{2+}-dependent ion channels TMEM16A and SK4 possibly by acting as a counterion channel. *Pflugers Arch*. 2010;459(3):485–497.
61. Jin X, et al. Activation of the Cl^- channel ANO1 by localized calcium signals in nociceptive sensory neurons requires coupling with the IP3 receptor. *Sci Signal*. 2013;6(290):ra73.
62. Jin X, Shah S, Du X, Zhang H, Gamper N. Activation of Ca(2+)-activated Cl(−) channel ANO1 by localized Ca(2+) signals. *J Physiol (Lond)*. 2016;594(1):19–30.
63. Maus M, et al. Missense mutation in immunodeficient patients shows the multifunctional roles of coiled-coil domain 3 (CC3) in STIM1 activation. *Proc Natl Acad Sci U S A*. 2015;112(19):6206–6211.
64. Courjaret R, Machaca K. Mid-range Ca^{2+} signalling mediated by functional coupling between store-operated Ca^{2+} entry and IP3-dependent Ca^{2+} release. *Nat Commun*. 2014;5:3916.
65. Caputo A, et al. TMEM16A, a membrane protein associated with calcium-dependent chloride channel activity. *Science*. 2008;322(5901):590–594.
66. Schroeder BC, Cheng T, Jan YN, Jan LY. Expression cloning of TMEM16A as a calcium-activated chloride channel subunit. *Cell*. 2008;134(6):1019–1029.
67. Yu K, Lujan R, Marmorstein A, Gabriel S, Hartzell HC. Bestrophin-2 mediates bicarbonate transport by goblet cells in mouse colon. *J Clin Invest*. 2010;120(5):1722–1735.
68. Rosenthal R, et al. Expression of bestrophin-1, the product of the VMD2 gene, modulates voltage-dependent Ca^{2+} channels in retinal pigment epithelial cells. *FASEB J*. 2006;20(1):178–180.
69. Ishikawa Y, Eguchi T, Skowronski MT, Ishida H. Acetylcholine acts on M3 muscarinic receptors and induces the translocation of aquaporin5 water channel via cytosolic Ca^{2+} elevation in rat parotid glands. *Biochem Biophys Res Commun*. 1998;245(3):835–840.
70. Inoue R, et al. Immunolocalization and trans-

location of aquaporin-5 water channel in sweat glands. *J Dermatol Sci*. 2013;70(1):26–33.
71. Song Y, Sonawane N, Verkman AS. Localization of aquaporin-5 in sweat glands and functional analysis using knockout mice. *J Physiol (Lond)*. 2002;541(pt 2):561–568.
72. Sato K, Nishiyama A, Kobayashi M. Mechanical properties and functions of the myoepithelium in the eccrine sweat gland. *Am J Physiol*. 1979;237(3):C177–C184.
73. Davis FM, et al. Essential role of Orai1 store-operated calcium channels in lactation. *Proc Natl Acad Sci U S A*. 2015;112(18):5827–5832.
74. Ambudkar IS. Calcium signalling in salivary gland physiology and dysfunction. *J Physiol (Lond)*. 2016;594(11):2813–2824.
75. Xing J, Petranka JG, Davis FM, Desai PN, Putney JW, Bird GS. Role of Orai1 and store-operated calcium entry in mouse lacrimal gland signalling and function. *J Physiol (Lond)*. 2014;592(5):927–939.
76. Somasundaram A, et al. Store-operated CRAC channels regulate gene expression and proliferation in neural progenitor cells. *J Neurosci*. 2014;34(27):9107–9123.
77. Oh-Hora M, et al. Dual functions for the endoplasmic reticulum calcium sensors STIM1 and STIM2 in T cell activation and tolerance. *Nat Immunol*. 2008;9(4):432–443.
78. Dassule HR, Lewis P, Bei M, Maas R, McMahon AP. Sonic hedgehog regulates growth and morphogenesis of the tooth. *Development*. 2000;127(22):4775–4785.
79. Bevensee MO, Apkon M, Boron WF. Intracellular pH regulation in cultured astrocytes from rat hippocampus. II. Electrogenic Na/HCO3 cotransport. *J Gen Physiol*. 1997;110(4):467–483.